MOLECULAR AND CELLULAR BIOLOGY, Jan. 2009, p. 357–377 Vol. 29, No. 2
0270-7306/09/$08.00+0 doi:10.1128/MCB.01385-08

Role of the Molybdoflavoenzyme Aldehyde Oxidase Homolog 2 in the Biosynthesis of Retinoic Acid: Generation and Characterization of a Knockout Mouse▽†

Mineko Terao,[1]# Mami Kurosaki,[1]# Maria Monica Barzago,[1]# Maddalena Fratelli,[1] Renzo Bagnati,[2] Antonio Bastone,[1] Chiara Giudice,[3] Eugenio Scanziani,[3] Alessandra Mancuso,[4,5] Cecilia Tiveron,[4,6] and Enrico Garattini[1]*

Laboratory of Molecular Biology, Department of Biochemistry and Molecular Pharmacology,[1] and Department of Environmental Health,[2] Istituto di Ricerche Farmacologiche Mario Negri, Via La Masa 19, 20156 Milan, Italy; Dipartimento di Patologia Animale, Igiene e Sanità Pubblica Veterinaria, Sezione di Anatomia Patologica Veterinaria e Patologia Aviare, Facoltà di Medicina Veterinaria, Università degli Studi di Milan, Via Celoria 10, 20133 Milan, Italy[3]; Centro Ricerca Sperimentale, Istituto Regina Elena, Via delle Messi d'Oro, 156, 00158 Rome, Italy[4]; Università Cattolica del Sacro Cuore, Largo Gemelli 8, 00168 Rome, Italy[5]; and European Brain Research Institute (E.B.R.I.), Rita Levi-Montalcini Foundation, Via del Fosso di Fiorano 64/65, 00143 Rome, Italy[6]

Received 3 September 2008/Returned for modification 28 September 2008/Accepted 26 October 2008

The mouse aldehyde oxidase AOH2 (aldehyde oxidase homolog 2) is a molybdoflavoenzyme. Harderian glands are the richest source of AOH2, although the protein is detectable also in sebaceous glands, epidermis, and other keratinized epithelia. The levels of AOH2 in the Harderian gland and skin are controlled by genetic background, being maximal in CD1 and C57BL/6 and minimal in DBA/2, CBA, and 129/Sv strains. Testosterone is a negative regulator of AOH2 in Harderian glands. Purified AOH2 oxidizes retinaldehyde into retinoic acid, while it is devoid of pyridoxal-oxidizing activity. *Aoh2*$^{-/-}$ mice, the first aldehyde oxidase knockout animals ever generated, are viable and fertile. The data obtained for this knockout model indicate a significant role of AOH2 in the local synthesis and biodisposition of endogenous retinoids in the Harderian gland and skin. The Harderian gland's transcriptome of knockout mice demonstrates overall downregulation of direct retinoid-dependent genes as well as perturbations in pathways controlling lipid homeostasis and cellular secretion, particularly in sexually immature animals. The skin of knockout mice is characterized by thickening of the epidermis in basal conditions and after UV light exposure. This has correlates in the corresponding transcriptome, which shows enrichment and overall upregulation of genes involved in hypertrophic responses.

Aldehyde oxidases (AOXs) (EC 1.2.3.1) are structurally conserved proteins belonging to the family of molybdoflavoenzymes along with xanthine oxidoreductase (XOR), the key enzyme in the catabolism of purines (25, 28). In their catalytically active form, both AOXs and XORs are dimers of identical subunits characterized by three conserved domains separated by nonconserved hinge regions (28). The amino-terminal 25-kDa domain contains two nonidentical 2Fe-2S redox centers. The flavin adenine dinucleotide binding region is located in the intermediate 45-kDa domain, while the substrate and the molybdopterin cofactor binding pocket reside in the carboxy-terminal 85-kDa domain (28). AOXs have broad substrate specificity, hydroxylating N-heterocycles or oxidizing aliphatic as well as aromatic aldehydes into the corresponding acids (35, 41, 42).

The primary structures of mammalian AOXs and XORs are more than 40% identical, and the two types of enzymes are evolutionary related. Most of the available data indicate that AOXs evolved from a primordial form of XOR through a series of gene duplication events (28). In mammals, the number of *AOX* genes is variable and species specific (25, 28, 37, 65). Rodents have four AOX genes (*Aox1*, *Aoh1*, *Aoh2*, and *Aoh3*) which are the products of asynchronous duplication events and cluster at a short distance from one another on the same chromosome (chromosome 1c1 in mice and chromosome 9 in rats) (Fig. 1). The *Aoh1*, *Aoh2*, and *Aoh3* genes are also known as *Aox3*, *Aox4*, and *Aox3l*, respectively, and are currently designated with the latter names in the NCBI database. (The designation of the four mouse AOX genes as *Aox1*, *Aox3*, *Aox4*, and *Aox3l* in the NCBI database is still provisional. As discussed in the work of Garattini et al. [25], the gene names adopted in the NCBI database are confusing. For this reason, we decided to adopt our original nomenclature throughout the text and refer hereafter to the four mouse AOX genes as *Aox1*, *Aoh1*, *Aoh2*, and *Aoh3*). The four loci code for equivalent numbers of structurally related products, which represent AOX isoenzymatic forms. The dog has two functional genes, the orthologs of rodent *Aoh2* and *Aoh3*, and two pseudogenes showing high similarity with *Aox1* and *Aoh1* (25). Finally, the human genome is endowed with a single functional gene

* Corresponding author. Mailing address: Laboratory of Molecular Biology, Istituto di Ricerche Farmacologiche Mario Negri, via La Masa 19, 20156 Milan, Italy. Phone: 39-02-39014533. Fax: 39-02-3546277. E-mail: egarattini@marionegri.it.

† Supplemental material for this article may be found at http://mcb.asm.org/.

# M.T., M.K., and M.M.B. contributed equally to this work.

▽ Published ahead of print on 3 November 2008.

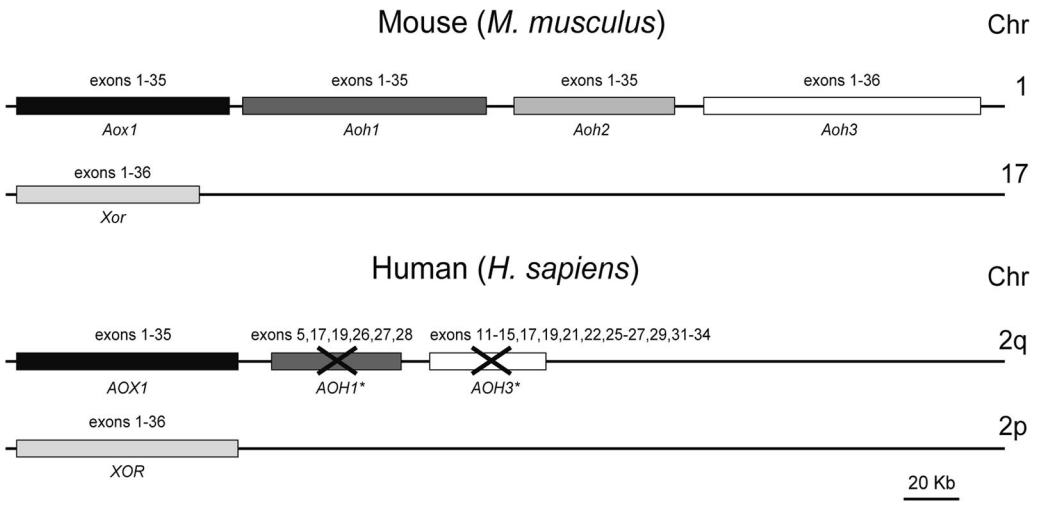

FIG. 1. The mouse and human AOX gene clusters and XOR locus. (Top) The lengths and relative positions of the four mouse AOX genes (*Aox1*, *Aoh1*, *Aoh2*, and *Aoh3*) mapping to chromosome 1 and the single XOR gene (*Xor*) on chromosome 17, along with their exon composition, are illustrated. (Bottom) The lengths and relative positions of the only functionally active human AOX gene (*AOX1*), the two pseudogenes *AOH1** and *AOH3** on chromosome 2q, and the XOR gene on chromosome 2p are shown. The exons present in the active mouse and human genes are indicated. The exons showing sequence similarity with the corresponding mouse orthologous genes are indicated above the two human pseudogenes. Chr, chromosome.

(*AOX1*) and two pseudogenes representing the vestiges of the mouse and rat *Aoh1* and *Aoh3* loci (28) (Fig. 1), all mapping to chromosome 2q (13, 28, 66).

Great amounts of human AOX1 as well as rodent AOX1 and AOX homolog 1 (AOH1) proteins are synthesized in liver and lung (2, 36, 46, 65–68), although cell-specific expression of these enzymes in other organs and tissues, such as the central nervous system, is observed (12, 13). Most of the data available on the function of these enzymes relate to hepatic AOXs and AOX1 in particular. This protein is a well-known drug-metabolizing enzyme, oxidizing various xenobiotics of medical and toxicological importance (6–11, 48–50, 53, 54). Expression of the *Aoh3* gene is restricted to the Bowman's gland, the main secretory organ of the nasal mucosa. The protein has been purified to homogeneity from this source and shown to have an overlapping set of substrates with AOX1 and AOH1 (31). No information is available on the product of the mouse *Aoh2* gene, whose protein has never been isolated. AOH2 orthologous proteins are predicted to exist in rats, marsupials, dogs, horses, and cows. It is possible that a functionally active *Aoh2* ortholog is also present in Old World monkeys, such as *Macaca* (M. Terao and E. Garattini, unpublished observations), although a similar gene is not found in chimpanzee and human genomes. The lack of *Aoh2* orthologs suggests a species-specific function that became dispensable in some primates and humans (23).

The physiological substrates of vertebrate AOXs are unknown, which makes it difficult to postulate a function for the enzymes. In vitro, all-*trans* retinaldehyde (RAL), the precursor of all-*trans* retinoic acid (ATRA), the active metabolite of vitamin A, is a good substrate for rat and mouse AOX1, AOH1, and AOH3. Other postulated endogenous substrates for AOXs are nicotinamide, pyridoxal, and serotonin oxidation metabolites (25). Finally, AOX activities have been implicated in the catabolism of the amino acids, isoleucine, leucine and valine (KEGG; http://www.kegg.jp).

The present article provides novel information on the tissue and cell distribution of the mouse AOH2 protein, demonstrating selective localization in the Harderian glands (HGs) and sebaceous glands as well as in keratinized epithelia. Purification and characterization of AOH2 demonstrate that the protein oxidizes RAL into ATRA with high affinity and efficiency. However, unlike AOH1 and AOX1 from different animals, mouse AOH2 is devoid of pyridoxal-oxidizing activity. Functional inactivation of the *Aoh2* gene by homologous recombination and generation of a knockout animal ($Aoh2^{-/-}$ mouse) demonstrates a deficiency of ATRA synthesis in both the HG and skin. This is accompanied by alterations in the phenotypes and transcriptomes of the two organs.

MATERIALS AND METHODS

Animals and treatments. Animals with different genetic backgrounds, namely, CD1, BDF1, C57BL/6, BDA/2, and 129/Sv, were purchased from Charles River Laboratories (Calco, Italy). Animals were maintained on standard chow and colonies expanded in standard-pathogen-free animal house facilities. All the procedures involving animals were performed according to the relevant national and international legislation and authorized by the internal Ethical Committee of the Animal Care Unit. Testosterone treatments were performed as described in a previous publication (36). To evaluate photodamage to the skin, female animals were shaved on the back and treated with UVB, using a light bulb placed at a 25-cm distance from the dorsal areas of the animal. Treatment consisted of a daily 30-min period of irradiation of anesthetized animals for 4 days. One hour after the last treatment, animals were sacrificed and extracted tissues were kept frozen until use. Tissue samples for the measurement of retinoids were prepared with minimal exposure to light.

Morphometric analysis of the skin. Four experimental groups were used for these studies: mock- and UV-treated wild-type (WT) and $Aoh2^{-/-}$ animals. Biopsy punches (8 mm in diameter) were obtained from the central part of the dorsal skin by use of a disposable apparatus (Stiefel Laboratories SRL, Milan, Italy). The biopsy samples were fixed in 4% paraformaldehyde and paraffin embedded and tissue sections were prepared according to standard protocols.

Five fields for each histological section (five slides per animal; four animals per experimental group) were randomly selected and the epidermal thickness was evaluated under the microscope (magnification, ×400). The epidermal thickness was expressed as the linear distance between the basal membrane and the apical portion of the last epithelial layer by use of an automatic image acquisition instrument (Image Pro Plus 4.5; Media Cybernetics). The minimal, maximal, mean, and median thicknesses of the epidermis were measured.

Generation of knockout mice. To prepare the targeting construct, a 1.3-kb EcoRI/NsiI genomic fragment derived from *Aoh2* intron 21 was cut from the PAC3 clone (67) and subcloned into the EcoRI/PstI sites of pBluescript (Stratagene, La Jolla, CA), and plasmid *pB1.3* was obtained. A 4.3-kb HindIII/BamHI genomic fragment consisting of *Aoh2* exons 23 to 26 and corresponding introns was subcloned into the HindIII/BamHI sites of pBluescript, and plasmid *pB4.3* was obtained. Plasmid *pB1.3* was digested with EcoRI/BamHI and inserted in the corresponding sites of the *pPNT* vector (47), and plasmid *pPNT1.3* was obtained. The 4.3-kb Aoh2 fragment contained in *pB4.3* was isolated by cleavage with XhoI/NotI and inserted in the corresponding sites of *pPNT1.3*, generating the entire targeting cassette. In this cassette, exon 22 was replaced by the neomycin resistance gene, the original NsiI and ScaI sites were eliminated, and a new XbaI site was derived from vector sequences.

The targeting vector was linearized by NotI digestion and electroporated in AB1 (129/Sv EvBrd$^-$ Hprt$^+$, kindly provided by Alan Bradley) embryonic stem (ES) cells according to standard procedures (33). Out of the 423 clones that were selected in the presence of the antibiotics G418 (Geneticin; Clontech, Palo Alto, CA) and FIAU (2′-fluoro-2′-deoxy-1-β-D-arabinofuranosyl-5-iodouracil; a kind gift from Eli-Lilly, Indianapolis, IN), only one clone, named 5E7, carried the homologous recombination event, as assessed by PCR and Southern blot analyses. Chimeric mice were generated by injection of 5E7 cells in the blastocoel cavity of 3.5-day BDF1 embryos (F_1 hybrids; C57BL/6 × DBA/2) (44). Upon maturity, chimeric animals bearing agouti hair were mated to C57BL/6 females, resulting in heterozygous animals with germ line transmission of the trait. Heterozygous *Aoh2* knockout mice were consecutively mated with C57BL/6 mice for nine generations to obtain an AOH2-deficient mouse line with a pure C57BL/6 background. The homogeneity of the background was confirmed by microsatellite analysis of the genome. Unless otherwise specified in the text, all the WT and knockout animals used for experiments were stabilized on the C57BL/6 genetic background.

Western blot analysis and in situ hybridization. Western blot analyses were performed as previously described using a chemiluminescence-based protocol (37, 68). The specific anti-AOX1, anti-AOH1, anti-AOH2, and anti-AOH3 rabbit polyclonal antibodies have also been described previously (37, 68). For the in situ hybridization experiments, a PCR-amplified fragment of AOH2 cDNA (nucleotides 4169 to 4787) was subcloned in pBluescript and used as the template for the synthesis of the sense and antisense riboprobes, employing T3 and T7 RNA polymerases (Stratagene), in the presence of ^{35}S-labeled thio-UTP (specific radioactivity, 1,200 Ci/mmol; GE Healthcare, Milan, Italy). Manipulation and hybridization of the probes to tissue sections were as described previously (68). Tissue sections were stained with hematoxylin-eosin and photographed under the microscope.

Measurements of RAL-oxidizing activity. RAL-oxidizing activity was determined in 100 μl of 10 mM of potassium phosphate buffer (pH 7.4) containing 15 to 100 μg of cytosolic protein extracts and 0.05 mM RAL, in the presence or absence of 2 mM NAD after incubation at 37°C for 10 min in the dark. The reaction was terminated by the addition of an equal volume of 95% butanol-5% methanol containing 0.005% butylated hydroxytoluene and centrifuged, and the supernatants were subjected to high-performance liquid chromatography (HPLC) analysis using a C_{18} reverse-phase column (70) or to mass spectrometric (MS) analysis (see Table S1 in the supplemental material).

Purification of mouse AOH2 protein, electrophoresis, and spectroscopy. Unless otherwise stated, all the purification steps were carried out at 4°C. HGs from 100 male mice (3.4 g) were homogenized in 8 volumes of 100 mM sodium phosphate buffer, pH 7.5, containing 0.2 mM phenylmethylsulfonyl fluoride, 1 μg/ml each of aprotinin and leupeptin, and 0.1 mg of soybean trypsin inhibitor, with an Ultraturrax homogenizer (IKA Werke GmbH, Staufen, Germany). Homogenates were centrifuged at 105,000 × *g* for 45 min to obtain cytosolic extracts. Extracts were heated at 55°C for 10 min and centrifuged at 15,000 × *g* to remove precipitated proteins. An equal volume of saturated ammonium sulfate was added to the supernatant, and the precipitate was collected by centrifugation at 15,000 × *g* and resuspended in 100 mM Tris-glycine buffer, pH 9.0. Solubilized proteins were mixed with 5 ml of benzamidine-Sepharose (Amersham Pharmacia Biotech, Uppsala, Sweden) preequilibrated in 100 mM Tris-glycine buffer, pH 9.0. Following 2 h of incubation, the resin was washed four times, each with 10 ml of the equilibration buffer to remove unbound proteins. Adsorbed proteins were eluted twice with 5-ml aliquots of equilibration buffer containing 5 mM benzamidine (Sigma Chemical Co., St. Louis, MO). The eluate was concentrated to ~1 ml with Centriplus YM-100 (Millipore Corp., Bedford, MA) and diluted to 10 ml with 50 mM Tris-HCl, pH 7.4. The solution was applied to a 5/5 fast protein liquid chromatography MonoQ (GE Healthcare) equilibrated in 50 mM Tris-HCl, pH 7.4. The AOH2 protein was eluted at 0.5 ml/min with a linear gradient (30 ml) from 0 to 1 M NaCl in 50 mM Tris-HCl, pH 7.4. The purification of AOH2 was monitored by determination of RAL-oxidizing activity and by quantitative Western blot analysis (37). One unit of enzymatic activity corresponds to 1 nmol of RAL oxidized/min. The absorbance spectrum of AOH2 in its native state was recorded at 20°C with a Hewlett-Packard HP8453 diode array spectrophotometer interfaced with a Vectra XA personal computer (Hewlett-Packard, Palo Alto, CA).

MS of the purified AOH2 protein. Electrospray ionization-tandem MS analyses of AOH2 tryptic peptides were performed according to standard protocols following in situ or in gel tryptic digestion using a Bruker Biflex matrix-assisted laser desorption ionization–time of flight (MALDI-TOF) MS (Bruker, Bremen, Germany) (37). Data generated were processed with the Mascot program (http://www.matrixscience.com) allowing a mass tolerance of 0.4 Da. Direct sequence analysis was carried out via collision-induced dissociation (CID) on an electrospray MS API 3000 (Applied Biosystems, San Diego, CA). The program MS-Tag (http://prospector.ucsf.edu) was used to correlate the experimental CID spectra to the theoretical CID spectra of tryptic peptides derived from proteins present in databases.

Whole-genome gene expression microarrays: collection of samples, experimental design, and analysis. For the studies involving HGs, WT and *Aoh2*$^{-/-}$ animals were divided into four groups: males and females before and after sexual maturation (5 to 6 and 7 to 9 weeks, respectively). Whole HGs were dissected without any contamination of surrounding tissues. At least three pairs of animals (WT and *Aoh2*$^{-/-}$) for each experimental group were used for the extraction of total RNA. When possible, each pair of age- and sex-matched RNA samples from WT and *Aoh2*$^{-/-}$ mice was obtained from siblings of the same heterozygous mating. Couples of samples were hybridized on the same slide, in dye-swapped duplicates, for a total of 30 microarrays. For the studies involving skin, equivalent biopsy samples (8 mm in diameter) of the dorsal areas of four WT and four *Aoh2*$^{-/-}$ female mice were obtained and processed for the extraction of RNA. Age-matched pairs of samples obtained from the same mating were hybridized on the same slide with a balanced dye design, for a total of eight microarrays.

All the experiments were performed with commercially available mouse gene expression microarrays consisting of approximately 44,000 probes (whole-mouse-genome microarray kit, 44,000 for the HG and 4 × 44,000 for the skin; Agilent, Palo Alto, CA). Total RNA was extracted using Qiagen RNeasy columns (Qiagen SpA, Milan, Italy). RNA (1 μg) was labeled with Cy3 or Cy5 by use of a commercially available kit (amino allyl message AmpII aRNA amplification kit; Ambion Inc., Austin, TX).

Microarray slides were scanned with an Agilent scanner, and image data were analyzed using the Feature Extraction software (Agilent, version 9.1). Due to the high variability between the *Aoh2*$^{-/-}$ and WT log ratios, we decided to perform variance stabilization normalization (VSN) (29). Two-way analysis of variance (ANOVA) was performed, with *Aoh2*$^{-/-}$ versus WT as the first factor and the four animal groups as the second factor. A total of 3,977 probes showed a *P* value of less than 0.005 for at least one of the factors or for their interaction. This corresponds to a false-discovery rate of 5.5%. From this list we removed replicate probes or probes for the same genes according to the following criteria: (i) a preference for probes with lower *P* values; (ii) when differences in *P* values were low, a preference for the probes significant for factor i; and (iii) a preference for probes corresponding to NM-labeled reference sequences followed by XM-, AK-, and BC-labeled sequences. This resulted in a list of 3,468 nonreplicate genes that were used for the principal component analysis (PCA). PCA plots provide a graphical representation of high-dimensional expression data in low dimensions. Throughout the study, only two (normally the first two, sometimes the third, when it was endowed with a better discriminating power) of the three components that account for the highest variation are shown. The similarity within a set of samples or experimental groups is indicated by physical proximity.

Gene set enrichment analysis (GSEA) was performed using the gene score resampling method of the ErmineJ software (38). We performed the analysis using the individual genes' *P* values of the knockout versus WT factor in two-way ANOVA. We obtained a list of 339 categories showing a *P* value of less than 0.001 (Benjamini Hochberg correction for multiple testing, corresponding to a raw *P* value of 0.0001). Due to the inherent characteristics of the gene ontology (GO) annotation, the list is highly redundant. Therefore, we selected the most informative categories according to the following criteria: (i) the smallest cate-

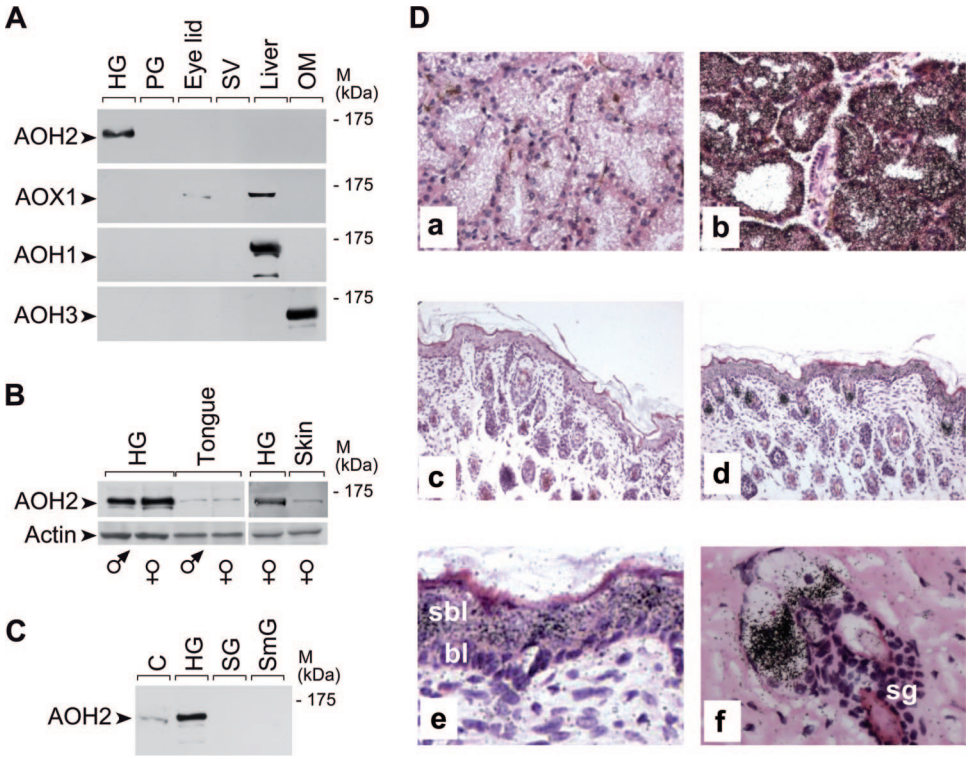

FIG. 2. Tissue- and cell-specific expression of the AOH2 protein and mRNA. (A, B, and C) Tissue and organ distribution of the AOH2 protein. Extracts (100 μg) of the indicated tissues and organs were loaded on an 8% polyacrylamide gel run in denaturing and reducing conditions, transferred to nitrocellulose membranes, and subjected to Western blot analysis with anti-AOH2, anti-AOX1, anti-AOH1, anti-AOH3, and anti-β-actin antibodies. Abbreviations: PG, preputial gland; SV, seminal vesicles; OM, olfactory mucosa; SG, salivary gland; SmG, submaxillary gland; C = extracts of HEK293 cells transfected with the full-length AOH2 cDNA used as a positive control for the experiment. (D) Tissue sections derived from HGs (a and b) and skin (c to f) were hybridized to a ^{35}S-radiolabeled AOH2 sense (a and c) or antisense (b, d, e, and f) riboprobes. Magnifications, ×200 (a and b), ×100 (c and d), and ×400 (e and f). Abbreviations: sbl, suprabasal layer; bl, basal layer; sg, sebaceous glands; M, molecular mass.

gory with the highest *P* value, (ii) preference for biological process categories over molecular function or cellular component, and (iii) selection of only one of the categories pertaining to the same group of biological processes. We used the same GSEA for two other gene categories that we considered important for our study and were not adequately represented in the GO database, namely, genes regulated by ATRA (5) and genes responsible for tissue hypertrophy (in the "diseases" lists of Metacore; http://www.genego.com). For the enriched pathways, we determined the general direction of the changes, performing GSEA and using log ratios rather than *P* values as scores. The same analysis was repeated twice, giving the best score to the highest log ratio (prevalence of upregulation) or, conversely, the best score to the lowest log ratio (prevalence of downregulation). We considered that there was a general downregulation if only downregulation analysis resulted in a significant difference ($P < 0.05$) or if there was a difference between downregulation and upregulation *P* values of more than 4 orders of magnitude.

The results of the microarray experiments performed on skin samples were normalized in two ways: (i) *lowess* normalization of the individual log ratios for the differential regulation analysis, and (ii) VSN for the comparison with the HG and for the PCA of the genes belonging to specific categories. GSEA was performed as described for the HG. After Benjamini Hochberg correction for multiple testing (corresponding to a raw *P* value of 0.0001), we obtained a list of 160 categories showing *P* values of less than 0.002.

Measurement of RAL and ATRA by MS. Reference standards of RAL and ATRA were from Sigma (St. Louis, MO). The internal standard (ST1926) is a synthetic retinoid and was synthesized by Sigma-tau Industrie Farmaceutiche Riunite S.p.A. (Pomezia, Italy). Stock solutions were made in acetonitrile at the concentration of 1 mg/ml and stored at −20°C in the dark. Working solutions containing all the substances to be analyzed were prepared before each analytical run. Acetonitrile for LC-MS was from Riedel de Haen (Seelze, Germany) and HPLC-grade Milli-Q water was obtained with a Milli-Ro Plus 90 apparatus (Millipore, Molsheim, France). The methodological details of the analytical procedure are described in Table S1 in the supplemental material.

Microarray data accession number. Further details on the design of the study and the methodologies used can be found under accession number GSE12541 of the GEO database, where the microarray data have been deposited (http://www.ncbi.nlm.nih.gov/geo/query/acc.cgi?token = rfohdqgwiqyywvo&acc = GSE12541).

RESULTS

AOH2 tissue- and cell-specific expression profile: high levels in the HGs and sebaceous glands with detectable levels in the epidermis and other keratinized epithelia. In a first set of experiments, we studied the tissue distribution of the AOH2 protein by Western blot analysis using an antipeptide polyclonal antibody devoid of cross-reactivity with other AOX isoenzymes (37). As shown in Fig. 2A, large amounts of AOH2 are synthesized by the HG, the major intraorbital exocrine gland located behind the ocular bulb. AOH2 is the only AOX present in this organ. The protein comigrates with the corresponding recombinant product expressed in HEK293T cells. This is in line with an apparent molecular mass of approximately 150 kDa and is consistent with the size of the putative monomeric subunit of mouse AOH2 (67, 68). The protein is also detectable in the skin, the mucosal layer lining the oral cavity (tongue) (Fig. 2B), and the esophagus (data not shown).

AOH2-negative tissues include kidney, adrenal gland, pancreas, hypophysis, brain, cerebellum, and spinal cord (data not shown). As indicated by Fig. 2C, AOH2 must serve a specific function in the HG, as the protein is not detectable in other exocrine structures such as the preputial, extraorbital lacrimal (data not shown), salivary, and submaxillary glands. The tissue distributions of AOH2 and other AOX isoenzymes differ. AOX1 and AOH1 are expressed predominantly in the liver (67), whereas AOH3 is restricted to the Bowman's gland in the nasal mucosa (Fig. 2A) (37). A strict correlation between the levels of AOH2 protein and corresponding mRNA is observed for the HG, tongue, esophagus, and skin, as assessed by Northern blot or quantitative reverse transcription-PCR (RT-PCR) analysis (data not shown).

The HG lays in close proximity with the intraorbital lacrimal gland, from which it cannot be dissected. The two structures can be recognized only at the microscopic level. The secretory acini of the HG are characterized by porphyrin deposits and lipid secretions inside the ductal lumen. In situ hybridization experiments with a specific antisense AOH2 RNA probe demonstrate that the corresponding transcript is expressed homogeneously and at high levels in the majority of the epithelial cell population lining the ducts of the HG (Fig. 2D, panel b). This is the predominant cell population present in the organ. No accumulation of silver grains is observed in vicinal tissue sections hybridized with the sense AOH2 RNA probe (Fig. 2D, panel a).

Further in situ hybridization experiments performed with the same AOH2 sense (Fig. 2D, panel c) and antisense (Fig. 2D, panel d) probes indicate that the low levels of AOH2 protein determined in the skin are the consequence of selective synthesis of the corresponding RNA in two locations: the epidermis and the sebaceous glands. Microphotographs of the epidermis taken at higher magnification (Fig. 2D, panel e) show that the AOH2 mRNA is synthesized only in the suprabasal layer, which differentiates from the basal layer of cells. This is similar to what observed for the keratinized epithelium covering the tongue, the esophagus, and the first part of the stomach (67). High-magnification pictures of the sebaceous glands (Fig. 2D, panel f) show accumulation of silver grains in the secretory epithelial cells, which are characterized by the production of a lipid-rich secretion similar to that of the HG.

Control of AOH2 expression in the HG by genetic background and testosterone. Interindividual variations in the levels of AOX have been reported for humans (25). Similarly, there is evidence of variability in the amounts of hepatic AOX activity in different mouse and rat strains via epigenetic mechanisms (25, 70). For mice, we observed epigenetic silencing of the AOH1 gene in certain common strains (70). Furthermore, mouse AOX1 and AOH1 show an expression profile which is dimorphic and gender dependent (36), as males synthesize larger amounts of hepatic AOX1 and AOH1 proteins than females (36). To establish the existence of variations in the expression of AOH2 in different animal strains, we considered four types of mouse. The outbred CD1 and the inbred C57BL/6 mice are proficient, while DBA/2 and CBA mice are deficient for the expression of hepatic AOH1 in the liver (70). In this study, we also included 129/Sv, since this is the strain of origin of the ES cell line used for the generation of the *Aoh2* knockout mice described below.

As expected, the HGs of C57BL/6 and CD1 mice are rich sources of AOH2 (Fig. 3A). Furthermore, the two strains synthesize detectable and equivalent amounts of the protein in the skin (Fig. 2B and 3B). In contrast, the HGs and the skin of DBA/2, CBA, and 129/Sv animals are devoid of AOH2 (Fig. 3A and B). Thus, DBA/2 and CBA strains have a general deficit in the tissue-specific synthesis of AOXs involving not only AOH1 and AOX1 but also AOH2. This is not the case for 129/Sv mice (64), which are not deficient in the expression of hepatic AOH1 and AOX1 (70).

To define whether AOH2 is regulated in a sex-specific manner by steroid hormones, we determined the steady-state levels of the protein in the HGs of male and female animals during the postnatal development of C57BL/6 mice. As illustrated in Fig. 3C, sexually immature animals (5 and 7 weeks), which are characterized by low circulating levels of steroid hormones, and fully mature mice (>13 weeks) show similar amounts of the AOH2 protein. Surprisingly, the HGs of 9-week-old males synthesize almost three times less AOH2 than females. Thus, there is a narrow temporal window during the postnatal development of the HG, in which AOH2 acts as a sexually dimorphic protein. Interestingly, maximal secretion of androgens is observed around the ninth week (31), a time which normally marks full sexual maturity of the male mouse. To assess whether androgens may be involved in the regulation of AOH2 synthesis, 6-week-old females were treated with testosterone for 2 weeks (Fig. 3D). Testosterone administration results in an approximately twofold reduction in the steady-state levels of the HG's AOH2 protein. This is the opposite to what observed in the case of hepatic AOX1 (36) and AOH1 (Fig. 3D), which are dramatically induced by the androgen.

Purification and biochemical characterization of the AOH2 protein from the HG. As a first step in the biochemical characterization of the AOH2 protein, we purified the enzyme to homogeneity from the HG. The recovery of purified AOH2 is approximately 5% with a purification factor of approximately 350-fold (Table 1). Both parameters compare well with the yield and purity of other catalytically active mammalian molybdoflavoenzymes (37, 67). Highly purified preparations of AOH2 consist of a single and symmetrical protein peak coeluting with anti-AOH2 immunoreactivity (Fig. 4A). The monomeric subunit of purified AOH2 consists of a single protein band with an apparent molecular mass of 150 kDa (Fig. 4B). A further characterization of AOH2 by MALDI-TOF analysis of the trypsin hydrolysate obtained from the purified protein is shown in Fig. 4C. As expected from the sequence data of the corresponding cDNA (36, 37, 67), the tryptic fingerprints of purified AOH2, AOX1, AOH1, and AOH3 are completely different. Comparison of the masses obtained experimentally and predicted from the open reading frame of the AOH2 cDNA allowed us to identify 73 tryptic peptides with a 59.6% sequence coverage of the AOH2 protein (see Table S2 in the supplemental material). Spectroscopic analysis of purified AOH2 shows the typical profile of a molybdoflavoenzyme characterized by a broad maximum of around 450 nm (Fig. 4D). The spectrum of AOH2 and that of purified mouse liver AOH1, which is shown for comparison, are indistinguishable.

Studies performed on purified AOH2 indicate that the enzyme is capable of oxidizing some of the exogenous substrates recognized by other mammalian AOXs (data not shown). As

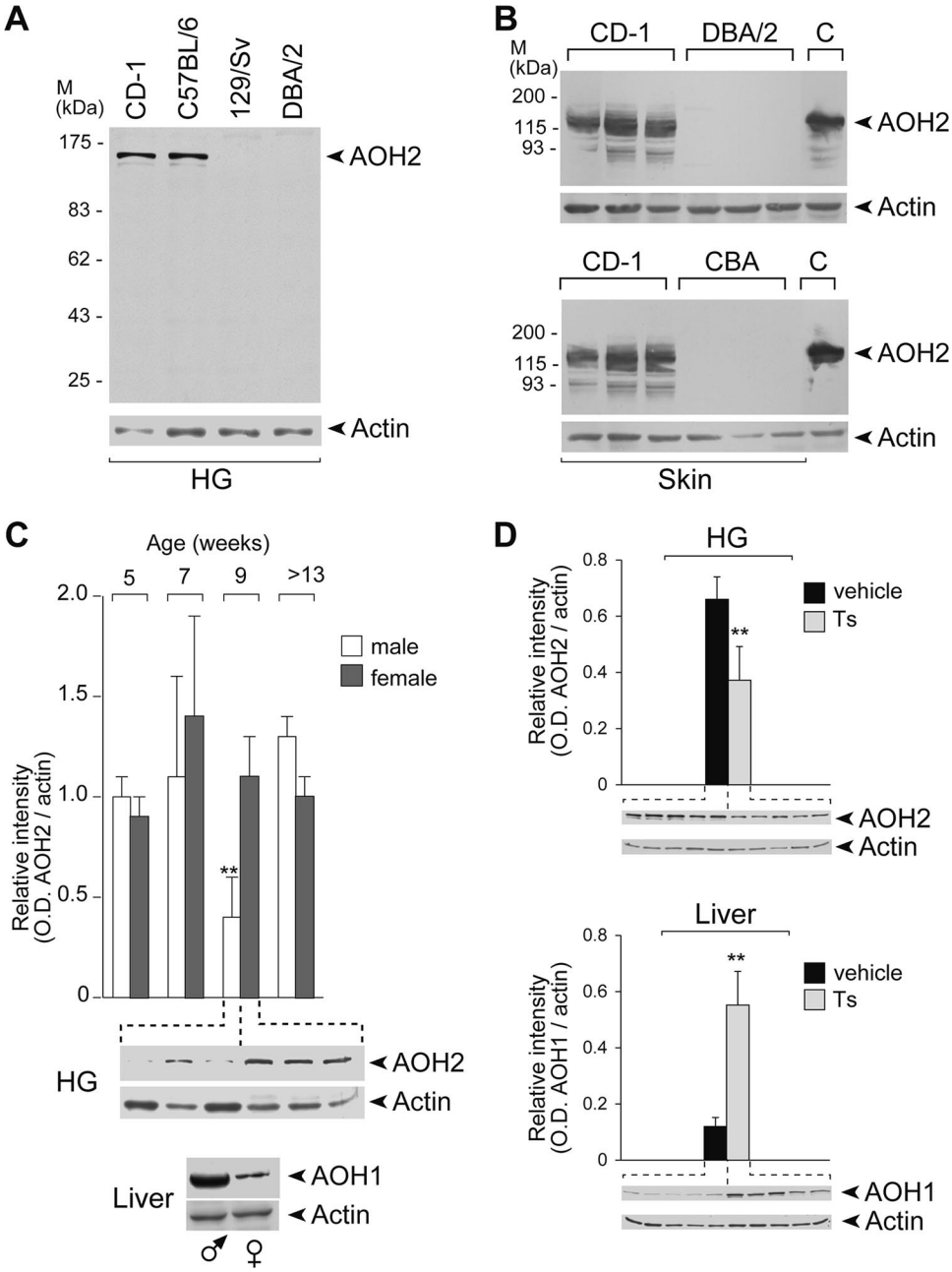

FIG. 3. Strain differences and hormonal regulation of AOH2. (A) Cytosolic extracts of HG were prepared from the indicated mouse strains and subjected to Western blot analysis (100 μg of proteins) using anti-AOH2 and anti-β-actin antibodies. (B) Cytosolic fractions of skin derived from the indicated mouse strains were treated at 55°C for 10 min and centrifuged to eliminate precipitated proteins. The supernatant was precipitated with 50% ammonium sulfate to enrich for AOH2. Concentrated extracts (100 μg of proteins) were subjected to Western blot analysis as in the left panel. C, extracts of HEK293 cells transfected with the full-length AOH2 cDNA used as a positive control of the experiment. (C) Cytosolic fractions were prepared from the HGs isolated from individual animals of the indicated ages and sexes (male [♂] and female [♀]). The extracts (50 μg of proteins) were subjected to Western blot analysis as for panel A. (Top) Bar graph summarizing the results obtained by densitometric analysis of all the blots; (middle) representative results obtained for 9-week-old animals; (bottom), for comparative reasons, typical results of a Western blot analysis conducted with anti-AOH1 antibodies in liver extracts are shown. **, significantly lower than the corresponding group of female animals (Student's t test; $P < 0.01$; $n = 3$). (D) Cytosolic extracts (50 μg) of the HG and liver derived from individual female animals treated with vehicle or testosterone propionate (Ts) were subjected to Western blot analysis with anti-AOH2 (HG), anti-AOH1 (liver), and anti-β-actin antibodies. The graphs summarize the results obtained by densitometric analysis of the blots illustrated. **, Significantly lower (HG) or higher (liver) than the corresponding vehicle-treated group (Student's t test; $P < 0.01$; $n = 3$). M, molecular mass.

to endogenous substrates, a major difference between AOH2 and other AOXs is the inability to recognize the vitamin B1 precursor, pyridoxal. Lack of oxidizing activity is observed at two substrate concentrations that are metabolized effectively by the same amount of purified mouse liver AOH1 (see Fig. S1A in the supplemental material). Similar to what was observed for AOH1, purified AOH2 oxidizes RAL into ATRA (see Fig. S1B in the supplemental material). The enzymatic

TABLE 1. Purification of AOH2 from HGs[a]

Step[b]	Vol (ml)	Protein amt (mg)	Activity (units)	Sp act (units/mg)	Fold purification	% Yield
Ultra	22	409	123.9	0.3	1	100
55°C	22	245	95.3	0.4	1.3	77
PD10	28	112	83.1	0.7	2.3	67
Benz. Seph.	15	0.33	NA	NA	NA	NA
MonoQ	1.4	0.06	6.2	103.8	346	5

[a] HGs (3.4 g) were isolated, homogenized in 27 ml of buffer, and ultracentrifuged to obtain a cytosolic extract, which was processed as indicated. Enzymatic activity was measured as the ability of the various purification fractions to oxidize RAL into ATRA. One unit of enzymatic activity is defined as 1 nmol of RAL oxidized/min. The results are representative of two separate AOH2 preparations. NA, not applicable.

[b] Ultra, ultracentrifugation; 55°C, treatment at 55°C; PD10, size exclusion column; Benz. Seph., benzamidine-Sepharose affinity column chromatography; MonoQ, MonoQ anion-exchange column chromatography.

reaction follows classic Michaelis-Menten kinetics (see Fig. S1C in the supplemental material), and the calculated K_m and V_{max} values of AOH2 are 4.8 μM and 0.06 μmol/min/mg of protein, respectively. These values are comparable with those calculated for AOX1 and AOH1 (66, 70). Our results demonstrate that RAL is an excellent substrate for all the members of the mouse AOX family.

Generation and characterization of animals with knockout of the *Aoh2* gene. To gain insights into the physiological function of AOH2, a specific knockout mouse (*Aoh2*$^{-/-}$) was generated. To delete the gene, a plasmid construct targeting exon 22 of the mouse *Aoh2* gene was introduced into ES cells (Fig. 5A). *Aoh2*$^{+/-}$ founder mice were identified in the F_1 progeny by genotyping and subsequently mated to obtain homozygous animals. The Southern blot analysis performed with 5′ and 3′ probes confirmed the specific targeting of *Aoh2* (Fig. 5B and Fig. C). The first generation of *Aoh2*$^{-/-}$ animals was obtained by microinjection of 129/Sv-derived ES cells into BDF1-derived blastocysts (BDF1 mice are an F_1 hybrid of C57BL/6 and DBA/2 mice), and the line was initially expanded in the same strain of mice. As described above, such a mixed genetic background was inappropriate for our studies on AOH2. For this reason, we rederived the *Aoh2*$^{+/-}$ heterozygous founders into the C57BL/6 background by nine consecutive backcrosses. The ninth-generation animals have a highly homogeneous C57BL/6 background, as assessed by microsatellite analysis (data not shown), and were used for all the subsequent studies.

Deletion of *Aoh2* exon 22 results in the disappearance of the corresponding transcript from the HGs of *Aoh2*$^{-/-}$ animals, as demonstrated by Northern blot analysis, by use of a full-length cDNA and an exon 22-specific probe (Fig. 5D). In the same experimental conditions, heterozygotes were characterized by an approximately 50% reduction in the levels of the AOH2 transcript, while the HGs and skin of homozygous knockout mice did not produce any AOH2 transcript or protein (Fig. 5E and F).

In spite of a complete lack of the molybdoflavoenzyme in target organs and tissues, *Aoh2*$^{-/-}$ animals do not show any macroscopic, structural, functional, or behavioral abnormality compared with the corresponding heterozygous and WT counterparts. The growth curves of *Aoh2*$^{-/-}$, *Aoh2*$^{+/-}$, and WT animals are superimposable. The frequency of the defective allele transmission is almost Mendelian. Heterozygous mating resulted in the birth of 839 siblings, with 21% *Aoh2*$^{-/-}$, 52% *Aoh2*$^{+/-}$, and 27% WT animals. The frequency of knockout mice in the progeny was slightly below the expected 25% ($P < 0.05$ after chi-square test), and the corresponding allele frequency in the population was lower than the expected 50%, suggesting a minor survival disadvantage of the animals carrying the mutated *Aoh2* trait. The numbers of female (424 [51%]) and male (415 [49%]) animals were not significantly different, indicating lack of sex biases.

Subtle alterations in the global gene expression profile of the *Aoh2*$^{-/-}$ HG: effect of sex and age. The functional development of HGs occurs predominantly after birth and is sexually dimorphic in terms of structure, biochemistry, and function (15). With this in mind, we sought for organ abnormalities in *Aoh2*$^{-/-}$ mice of both genders. Although AOH2 is controlled by testosterone during a defined period of the HG postnatal development (Fig. 3C), the protein does not seem to play a significant role in shaping the architecture of the gland in either male or female mice. As expected, adult C57BL/6 WT males were characterized by HGs slightly heavier and larger than those of females. However, the glands of *Aoh2*$^{-/-}$ and WT male or female animals do not show any difference in microscopic appearance.

Seeking perturbations of specific biochemical pathways and cellular processes caused by the absence of AOH2, we compared the global gene expression profiles in the HGs of WT and *Aoh2*$^{-/-}$ male and female animals before and after sexual maturation. Two-way ANOVA of the microarray intensity data with AOH2 deletion used as the first factor and the four experimental groups as the second one resulted in the selection of 3,468 significantly perturbed genes (see Materials and Methods). PCA of these selected data indicates that there is a remarkable variation of gene expression in the HGs of WT animals (Fig. 6A). Our results indicate that age is a primary determinant of the transcriptome, as indicated by the distance of the dots. This is in line with the idea that the full functional development of the gland occurs predominantly after birth (14). Major differences in the gender-specific complement of genes expressed in WT animals are observed as well. While sex and age have a dramatic impact on the variability of gene expression, the absence of AOH2 has a limited effect.

At the single-gene level, Fig. 6B shows the small number of genes up- or downregulated by AOH2 deficiency. Significantly, most of the induced changes are observed in sexually immature mice. This suggests that AOH2 function is particularly significant during the maturation of HGs. The vast majority of the up- or downregulated genes are the same in both immature female and male animals. *Sgpl1* (NM_009163), coding for sphingosine-1-phosphate lyase, is at the top of the list of upregulated genes. *Sgpl1* is involved in the degradation of sphingosine-1-phosphate, which regulates the proliferation of mammalian cells in a negative fashion (61). *Ncaph2* (NM_025795) and *Raf1* (NM_029780) are other genes involved in the control of cell proliferation that are upregulated in *Aoh2*$^{-/-}$ animals. The presence of *Acsl6* (NM_144823, coding for acyl coenzyme A synthetase long-chain family member 6) and *Elovl1* (NM_019422, coding for elongation of very-long-chain fatty acids), whose protein products are involved in lipid biosynthesis, is also of interest.

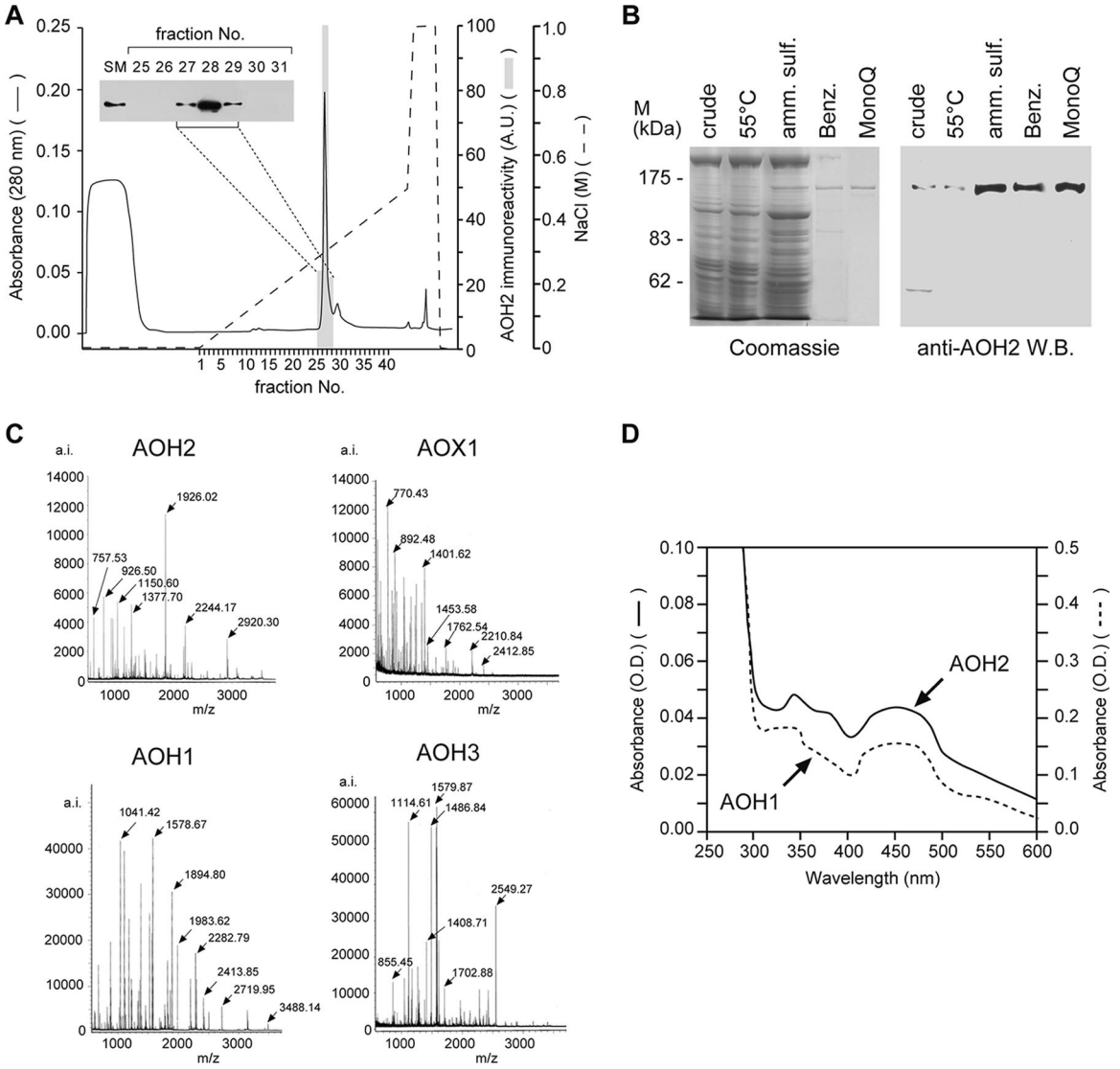

FIG. 4. Purification and characterization of the AOH2 protein from HGs. (A) The protein fraction (330 μg) purified from benzamidine-Sepharose was applied on a MonoQ fast protein liquid chromatography column and eluted with a linear gradient of NaCl, as indicated (dashed line). The column was run at a flow rate of 0.5 ml/min, and 2-ml fractions were collected. An aliquot of each chromatographic fraction was assayed for AOH2 immunoreactivity by quantitative Western blot analysis, and the corresponding elution profile is indicated by the shaded columns superimposed over the protein elution profile monitored at 280 nm. The inset shows the results of the Western blot performed on aliquots of the indicated chromatographic fractions using the anti-AOH2 antibody. Abbreviations: SM, starting material; A.U., arbitrary units. (B) Coomassie blue protein staining, following polyacrylamide gel electrophoresis (left) or Western blot analysis (right), of the indicated protein preparations obtained at various steps in the purification procedure are shown. "Crude" indicates supernatant centrifuged at 105,000 × *g*; "55°C" indicates supernatant following heat treatment at 55°C for 10 min. Abbreviations: amm. sulf., ammonium sulfate precipitate; Benz., eluate from benzamidine-Sepharose affinity column chromatography; MonoQ, eluate from MonoQ anion-exchange column chromatography; M, molecular mass. (C) AOH2 purified from the HG was trypsinized and subjected to MALDI-TOF analysis. The fingerprint mass spectra of purified AOH2, AOX1 (from livers of DBA/2 mice), AOH1 (from livers of CD1 mice), and AOH3 (from the nasal mucosae of CD1 mice) are compared. (D) Absorbance spectra of purified AOH2 and AOH1 in native conditions. O.D., optical density.

Noticeably, the AOH2 transcript was dramatically downregulated by more than eightfold in *Aoh2*$^{-/-}$ animals across all the experimental conditions considered. To further validate the results of our analysis, we selected four genes at random (*Spt1*, NM_009267; *Pip*, NM_008843; *Myh4*, NM_010855; and *Ckmt2*, NM_198415) and amplified the corresponding transcript by quantitative real-time RT-PCR with the same RNA preparations used for the microarray experiments. Comparison of the intensity data obtained by RT-PCR and microarray analyses demonstrates an excellent correlation (see Fig. S2A in the supplemental material).

Gene pathways altered in the HGs of *Aoh2*$^{-/-}$ mice: lipid homeostasis, cell secretion, and tissue remodeling. Due to the small effect of AOH2 deletion, in terms of both the number of affected genes and the changes in intensity, we performed a pathway analysis (see Materials and Methods). Among the GO categories showing statistically significant enrichment, we selected the smallest and most significant gene sets,

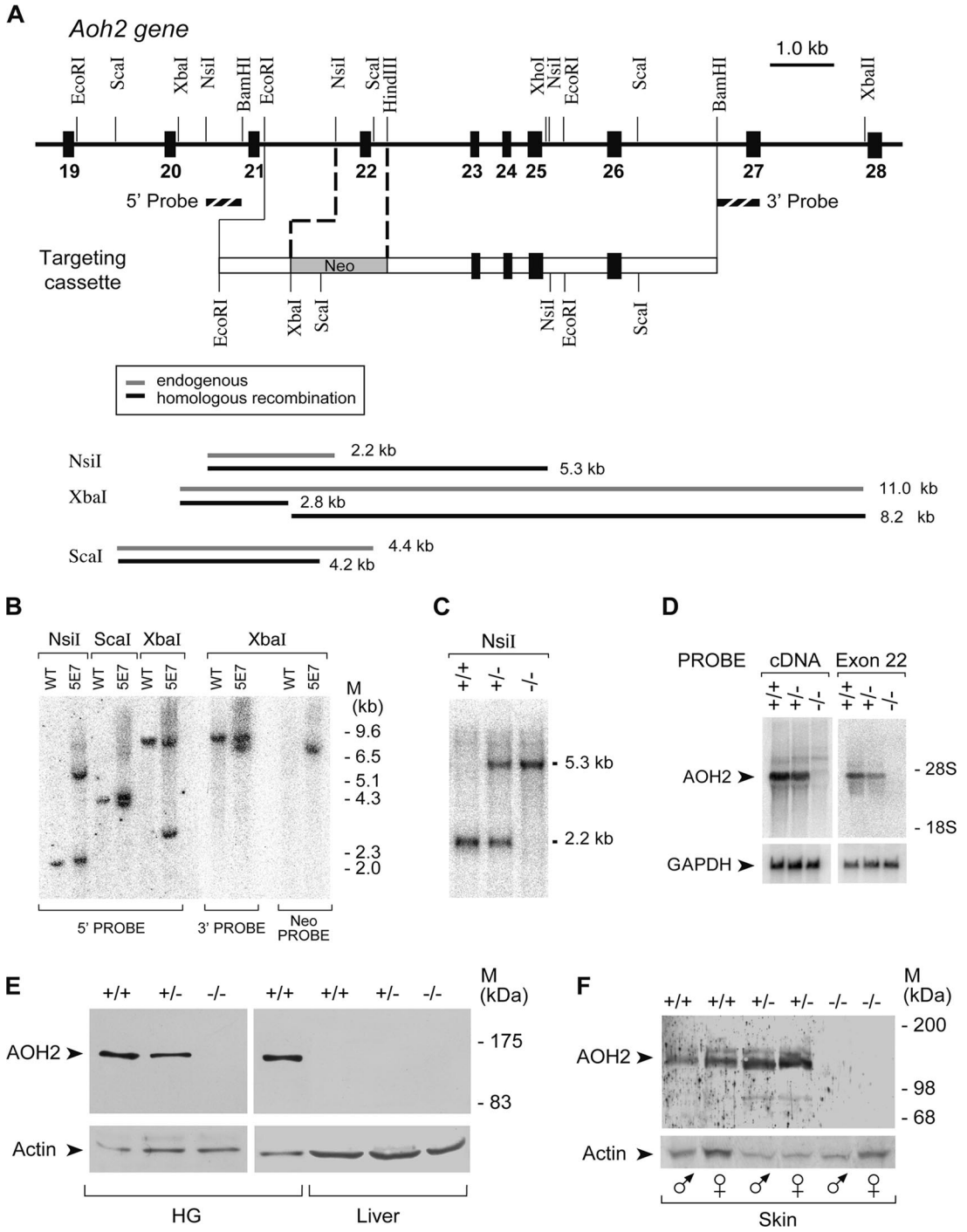

FIG. 5. Generation of *Aoh2*$^{-/-}$ mice. (A) (Top) A schematic representation of the targeting cassette used for homologous recombination is illustrated below the corresponding region of the *Aoh2* gene. The 5′-to-3′ orientation is from left to right. Exons and introns are represented by black and white boxes, respectively. In the targeting cassette, the neomycin resistance gene (Neo) is inserted in place of exon 22 and substitutes the corresponding genomic region of the *Aoh2* locus upon homologous recombination. Selected restriction endonuclease sites relevant for the construction of the targeting vector and the detection of the homologous recombination event are listed. The position of the probes (dashed boxes) used for the detection of homologous recombination by Southern blotting are also shown. (Bottom) The sizes of the restriction fragments before and after homologous recombination are schematically represented. (B) The Southern blot analyses of genomic DNA isolated from the ES cell clone (5E7) showing homologous recombination at the *Aoh2* locus and parental ES cell line (WT), with the indicated probes, are compared. (C) Germ line transmission of the homologous recombination event was confirmed by the Southern blot analysis shown and performed on DNA isolated from WT (+/+) and heterozygous (+/−) and homozygous (−/−) *Aoh2*$^{-/-}$ animals. (D) Northern blot analysis on total RNA derived from the HGs of WT (+/+) and heterozygous (+/−) and homozygous (−/−) *Aoh2*$^{-/-}$ animals, with a full-length AOH2 cDNA or an exon 22-specific probe, as indicated. The blot was rehybridized with GAPDH (glyceraldehyde-3-phosphate dehydrogenase) to ascertain that equal quantities of RNA were loaded in each lane. (E) Western blot analyses of cytosolic extracts (50 μg of protein) obtained from the HG and livers of male WT (+/+), heterozygous (+/−), and homozygous (−/−) *Aoh2* animals. (F) AOH2-enriched skin protein extracts (100 μg of protein) obtained as for Fig. 3A from male (♂) and female (♀) WT (+/+), heterozygous (+/−), and homozygous (−/−) *Aoh2* animals were subjected to Western blot analysis. All the blots were developed following incubation with anti-AOH2 and anti-β-actin antibodies. M, molecular mass.

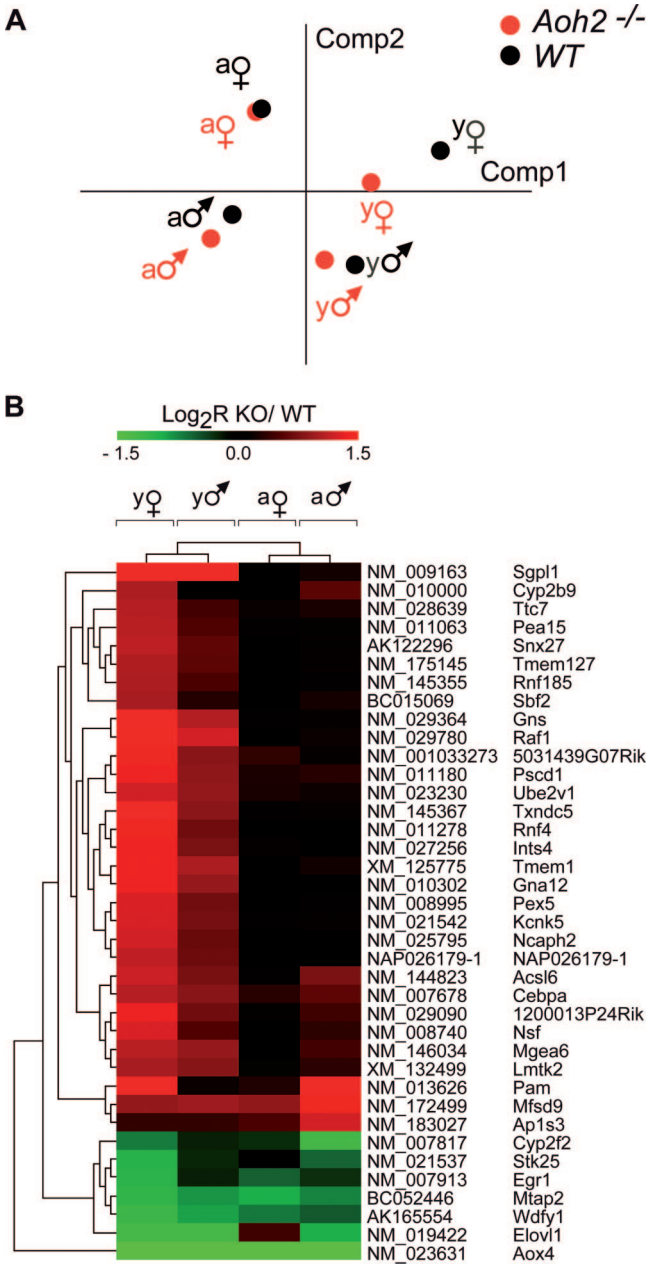

FIG. 6. Alterations in the transcriptome of the HGs: effects of age, sex, and *Aoh2* deletion. The gene expression data obtained with the use of whole-genome microarrays were analyzed after stratification for sex, age, and *Aoh2* deletion. (A) The PCA of the VSN intensity values (means centered) of the 3,468 genes that were significant for any of the factors ($Aoh2^{-/-}$ versus WT, age/sex groups, or interaction) after two-way ANOVA in the eight experimental groups. Comp, component. (B) Genes that were most significantly affected by AOH2 deletion ($P < 0.001$ for the "knockout" (KO) factor after two-way ANOVA and ≥2-fold change in at least one of the four groups). Genes and samples were clustered using Euclidean distance and average linkage. According to PCA, young animals cluster together, and show similar changes, while minimal changes are apparent in mature animals. Symbols: ♂, male; ♀, female. Abbreviations: a, adult; y, young.

reducing the redundancy which is inherent to the GO annotation (Table 2).

Ablation of the *Aoh2* gene results in a significant enrichment of pathways controlling two of the main functions exerted by the gland, i.e., lipid synthesis/catabolism (GO:0008610; GO:0016042) and cellular absorption/secretion (GO:0016192; GO:0045045; GO:0006897 GO:0048193). In the context of cellular secretion, besides pathways controlling endocytosis and Golgi vesicle transport, the presence of the pathway *ATPase activity* (GO:0016887), consisting predominantly of genes encoding ATP-dependent ATP-binding cassette (ABC) transporters, is of particular relevance. In fact, human AOX1 has been recently demonstrated to interact specifically with a member of the ABC transporter family (64). Given the structural similarity with AOX1, it is possible that AOH2 is also capable of interacting with one or more ABC transporters. Suppression of this interaction in the HGs of $Aoh2^{-/-}$ animals may cause the observed reorientation of the ATPase activity pathway in an attempt to compensate for the deficit. Given the role exerted by the ABC transporters and AOX1 (72) in the absorption/secretion of lipids, this may be linked to the observed perturbations in the lipid biosynthetic pathways.

AOH2 deletion also seems to have a major impact on the process of tissue remodeling. In fact, a first large group of interconnected pathways significantly enriched in $Aoh2^{-/-}$ animals controls cell proliferation and cell death/survival (GO:0008285, GO:0000082, GO:0043065, GO:00443069, and GO:0008637). This may be linked to the enrichment of stress-response pathways (GO:0006974, GO:0009611, GO:0006800), including ubiquitin-dependent proteolysis (GO:0006511) and maintenance of chromatin architecture (GO:0006325). A second group of enriched pathways control cell-cell and cell-matrix adhesion (GO:0007160 and GO:0007229), cell projection (GO:0042995), and cell migration (GO:0016477), and these pathways are also linked to tissue remodeling. All these pathways are known to control the homeostasis of the cytoskeleton. Thus, it may not be surprising that group of genes controlling actin polymerization/organization (GO:0030036) and microtubule assembly (GO:0000226) are also affected by *Aoh2* deletion. Perturbations in the gene networks involved in general cellular processes such as the regulation of transcription (GO:0045892, GO:0045893), nuclear mRNA splicing (GO:0000398), glucose catabolism (GO:0006007), or protein translation (GO:0006413) may simply reflect nonspecific responses to tissue- and cell-remodeling clues. Our analysis indicates also perturbation of specific signal transduction systems controlling the proliferation/apoptosis of epithelial cells, such as the Wnt and Rho pathways (GO:0016055, GO:0007266).

RAL-oxidizing activity in the $Aoh2^{-/-}$ animal: role of AOH2 in the HG and skin. RAL, the precursor of ATRA, the vitamin A active metabolite, is an excellent substrate for purified AOH2 (see Fig. S1B and S1C in the supplemental material). Thus, we deemed it interesting to evaluate whether AOH2 is a significant modulator of the vitamin A system in the HG and to conduct similar studies for the skin. RAL is a potential substrate of AOH2 but is also a recognized substrate of at least three RAL dehydrogenases (RALDHs) known as Raldh1, Raldh2, and Raldh3 (45). Like AOH2, RALDHs are cytosolic enzymes; however, unlike AOXs, they require NAD^+ as a cofactor in the oxidation of RAL into ATRA (43).

As a first approach, we determined the level of RAL-oxidizing activity in extracts of the HGs from WT and $Aoh2^{-/-}$ animals. Cytosolic fractions were first depleted of NAD^+ on size exclusion columns. Subsequently, these fractions were in-

TABLE 2. GO categories significantly perturbed in HGs and skin of *Aoh2*$^{-/-}$ mice[a]

GO ID	Description	No. of:		HG		Skin	
		Probes	Genes	*P* value	Direction	*P* value	Direction
GO:0030036	**Actin cytoskeleton organization and biogenesis**	**191**	**89**	**1.00E–13**		**5.71E–06**	**UP**
GO:0000226	Microtubule cytoskeleton organization and biogenesis	54	30	1.00E–13	UP		
GO:0007017	Microtubule-based process	239	116			2.36E–05	UP
GO:0016459	Myosin complex	88	42	1.00E–13	DN		
GO:0007517	Muscle development	124	60	1.75E–07	DN		
GO:0016311	**Dephosphorylation**	**232**	**108**	**1.00E–13**	**UP**	**5.06E–08**	**UP**
GO:0007243	**Protein kinase cascade**	**112**	**65**	**1.00E–13**	**DN**	**1.40E–05**	**UP**
GO:0006469	Negative regulation of protein kinase activity	35	18			1.00E–12	DN
GO:0007266	**Rho protein signal transduction**	**122**	**54**	**1.00E–13**		**2.47E–05**	**UP**
GO:0016055	**Wnt receptor signaling pathway**	**174**	**100**	**6.58E–06**	**DN**	**1.31E–04**	**UP**
GO:0006511	**Ubiquitin-dependent protein catabolic process**	**213**	**98**	**1.00E–13**	**UP**	**7.46E–07**	**UP**
GO:0006457	**Protein folding**	**362**	**198**	**1.00E–13**	**UP**	**3.24E–09**	**UP**
GO:0009072	Aromatic amino acid family metabolic process	16	13			1.00E–12	
GO:0042136	Neurotransmitter biosynthetic process	16	11			1.00E–12	
GO:0008610	Lipid biosynthetic process	153	94	1.00E–13			
GO:0016042	Lipid catabolic process	83	56	7.40E–10	DN		
GO:0016192	**Vesicle-mediated transport**	**379**	**187**	**1.00E–13**	**UP**	**5.21E–10**	**UP**
GO:0045045	**Secretory pathway**	**215**	**101**	**2.60E–12**	**UP**	**3.63E–07**	**UP**
GO:0006897	**Endocytosis**	**212**	**112**	**1.00E–13**		**9.74E–07**	**UP**
GO:0048193	**Golgi vesicle transport**	**128**	**63**	**2.28E–11**	**UP**	**2.23E–06**	**UP**
GO:0007160	Cell-matrix adhesion	88	49	1.42E–08	DN		
GO:0007229	Integrin-mediated signaling pathway	149	74	3.44E–05	DN		
GO:0042995	**Cell projection**	**272**	**127**	**1.00E–13**	**UP**	**1.74E–06**	**UP**
GO:0016477	**Cell migration**	**348**	**174**	**1.00E–13**		**1.30E–05**	**UP**
GO:0001525	Angiogenesis	155	87	2.83E–12	DN		
GO:0030890	Positive regulation of B-cell proliferation	16	9			1.00E–12	DN
GO:0050871	Positive regulation of B-cell activation	26	15			1.00E–12	DN
GO:0050671	Positive regulation of lymphocyte proliferation	31	17			1.00E–12	DN
GO:0007050	Cell cycle arrest	59	30			1.00E–12	DN
GO:0008285	**Negative regulation of cell proliferation**	**124**	**70**	**1.99E–10**	**UP**	**1.82E–12**	**UP**
GO:0000082	G_1/S transition of mitotic cell cycle	47	23	1.60E–04			
GO:0043065	Positive regulation of apoptosis	163	84	6.21E–09	DN		
GO:0043068	Positive regulation of programmed cell death	73	34			1.00E–12	UP
GO:0043069	**Negative regulation of programmed cell death**	**75**	**36**	**1.54E–13**	**UP**	**4.21E–10**	**UP**
GO:0008637	Apoptotic mitochondrial changes	28	15	1.00E–13	DN		
GO:0006325	**Maintenance of chromatin architecture**	**254**	**111**	**1.00E–13**	**UP**	**2.60E–10**	**UP**
GO:0045893	**Positive regulation of transcription, DNA dependent**	**308**	**168**	**1.00E–13**	**UP**	**1.24E–05**	**UP**
GO:0045892	**Negative regulation of transcription, DNA dependent**	**246**	**134**	**3.13E–12**	**DN**	**1.37E–08**	**UP**
GO:0006413	**Translational initiation**	**85**	**38**	**1.00E–13**	**UP**	**2.69E–05**	**UP**
GO:0000398	**Nuclear mRNA splicing, via spliceosome**	**229**	**117**	**1.00E–13**	**UP**	**5.93E–08**	
GO:0007283	Spermatogenesis	192	108	7.03E–06	UP		
GO:0048534	Hematopoietic or lymphoid organ development	75	42	6.53E–05	UP		
GO:0006974	**Response to DNA damage stimulus**	**294**	**159**	**8.44E–10**	**UP**	**1.00E–12**	
GO:0009611	Response to wounding	164	109	2.29E–04	UP		
GO:0009411	Response to UV	19	11			1.00E–12	
GO:0006800	Oxygen and reactive oxygen species metabolic process	58	43	3.12E–04			
GO:0015992	Proton transport	85	49	5.11E–05	UP		
GO:0006007	Glucose catabolic process	78	45	9.56E–10	UP		
GO:0019885	Antigen processing and presentation via MHC class I[b]	21	11			3.20E–04	
GO:0030216	Keratinocyte differentiation	21	11			3.20E–04	UP
GO:0016757	Transferase activity, transferring glycosyl groups	291	173	1.00E–13	DN		
GO:0004497	Mono-oxygenase activity	153	102	1.00E–13			
GO:0008146	Sulfotransferase activity	57	39	8.75E–03	DN		
GO:0015291	Porter activity	259	156	1.96E–10	DN		
GO:0020037	Heme binding	164	106	1.00E–13			
GO:0008168	**Methyltransferase activity**	**220**	**126**	**8.27E–09**		**1.15E–09**	**UP**
GO:0016712	Oxidoreductase activity, reduced flavin or flavoprotein	51	33	3.48E–11	DN		
GO:0016714	Oxidoreductase activity, reduced pteridine	7	6			1.00E–12	
GO:0016887	**ATPase activity**	**147**	**72**	**1.00E–13**	**UP**	**7.17E–05**	**UP**

[a] Following GSEA, we obtained two lists (HG and skin) of categories showing *P* values of less than 0.001 that were further reduced to eliminate redundancy, as detailed in Materials and Methods. Boldface indicates cases where the same pathways are enriched in both HGs and skin. In the case of the HG, up- or downregulation of the pathways was first determined in each of the four experimental groups (male and female; young and adult). The overall direction was considered as upregulation (UP) if the number of groups showing upregulation exceeded the number of groups characterized by downregulation. The opposite is true in the case of a downregulation (DN) notation.

[b] MHC, major histocompatibility complex.

cubated with RAL before and after readdition of the nicotinamide cofactor (Fig. 7A). We used liver extracts, which do not contain AOH2, as a comparison for our studies. In the HGs of WT animals, almost all the cytosolic RAL-oxidizing activity did not require NAD^+ and was due to AOH2. In fact, RAL-oxidizing activity was at the limit of detection in both NAD^+-depleted and NAD^+-repleted cytosolic extracts from the HGs of *Aoh2*$^{-/-}$ mice. Similar results were obtained with a conventional HPLC methodol (Fig. 7A) and a sensitive MS method (data not shown).

The same methodological approach was used for skin cytosolic extracts. In the absence of NAD^+, this tissue contains RAL-metabolizing activity approximately sevenfold lower than that seen for the HG, and the enzymatic activity can be measured only by MS. The readdition of NAD^+ causes an approximate and consistent 20% increase in RAL-oxidizing activity. This indicates that approximately 80% of the RAL transformed into ATRA is due to NAD^+-independent RAL oxidase(s). However, only 20% of this NAD^+-independent activity, which amounts to approximately 1 to 1.5 pmol/min/mg of protein, is due to AOH2, as indicated by the results obtained with the skin of *Aoh2*$^{-/-}$ mice. The remaining activity is likely to be contributed by the AOX1 isoenzyme, as determined for the skin by Western blot analysis (Fig. 8A).

The liver is the tissue that contains the highest levels of RAL-oxidizing activity by far. Approximately 85% of the total activity is NAD^+ dependent, indicating that RALDHs contribute the majority of RAL-oxidizing activity (43). In line with the absence of AOH2 protein in this organ (Fig. 2), hepatic extracts of WT and *Aoh2*$^{-/-}$ mice are characterized by similar amounts and proportions of NAD^+-dependent and NAD^+-independent RAL-metabolizing activity. Our observations indicate that AOH2 is the major RAL-metabolizing activity in the HG and contributes a significant amount of the same activity in the skin. The data presented were obtained from female animals, and similar results were observed for the male counterparts (data not shown).

We established the relevance of AOH2 for the oxidation of RAL in the whole organism by using sexually mature WT and *Aoh2*$^{-/-}$ mice. To this purpose, we set up a sensitive and specific MS method for the determination of RAL and ATRA. Figure S3 in the supplemental material contains representative chromatograms illustrating the amounts of RAL and ATRA in the HG. As illustrated in Fig. 7B, the glands of *Aoh2*$^{-/-}$ animals contain significantly lower amounts of ATRA than the WT counterparts. The absolute amounts of RAL in the HG are approximately 10-fold lower than the corresponding ATRA values and often at the detection limits of the assay. Nevertheless, in the same cohort used for the determination of RAL, we observed that *Aoh2*$^{-/-}$ animals were characterized by levels of RAL higher than those seen for WT mice. This is consistent with a significant role of AOH2 in the oxidation of RAL into ATRA.

We evaluated whether the observed effect could be generalized to the skin. Even in this second AOH2 target tissue, the content of ATRA is inferior in *Aoh2*$^{-/-}$ animals compared to that in WT animals. RAL in this organ is always below the detection limit. Noticeably, despite significant differences in the overall contributions of AOH2 to the total RAL-metabolizing activity in the skin and HG, the diminutions of ATRA in both organs are of the same order of magnitude.

ATRA controls the activity of numerous genes via interaction with specific nuclear receptors, which act as ligand-dependent transcription factors (18). However, only a limited set of retinoid-responsive genes are established and direct targets (5). The expression profile of this set of 29 genes was evaluated in the HGs of WT and *Aoh2*$^{-/-}$ mice by use of the microarray data set. We assessed the enrichment for the retinoid receptor signaling pathway in the four experimental groups of young and adult male or female *Aoh2*$^{-/-}$ animals. PCA demonstrated a clear separation of the dots corresponding to *Aoh2*$^{-/-}$ and WT animals regardless of the stratification for sex and age (Fig. 7C). Relative to the WT counterparts, a significant downregulation of the entire pathway ($P < 0.02$) was observed for female mice as well as for sexually mature *Aoh2*$^{-/-}$ male animals (Fig. 7D). The two genes whose levels were reduced most significantly in knockout relative to WT animals are *Egr1* (early growth response 1) and the gene for the ATRA-catabolizing enzyme *Cyp26b1* (cytochrome P450 26 b1). The expression of the two genes was evaluated by PCR analysis of the corresponding transcripts (see Fig. S2B in the supplemental material). This independent analysis confirmed the results obtained with the microarrays.

Substantial alterations in the global gene expression profile of the *Aoh2*$^{-/-}$ skin. Potential alterations in the skin transcriptome of the *Aoh2*$^{-/-}$ mice were studied only for sexually mature females to avoid variability due to age. The overall effect of AOH2 deletion in this organ was quantitatively more pronounced than that seen for the HG. As shown in Table 3), the deletion of AOH2 caused upregulation of a relatively large number of genes (68 genes were upregulated twofold or more; $P < 0.005$), while the number of downregulated genes (24 genes were downregulated twofold or more; $P < 0.005$) was limited. The physiological function of a substantial fraction of genes (37%) is unknown or ill defined.

The top upregulated gene is *Mtap2* (AK048375), which codes for an uncharacterized microtubule-associated protein. Second on the list is *Rps18* (AK018004), which is an 18S ribosomal protein. A substantial increase in two genes involved in lipid biosynthesis, *Elovl7* (NM_029001; *elongation of long chain fatty acids*) and *Lpgat1* (NM_172266; *lysophosphatidylglycerol acyltransferase 1*), is also remarkable. In line with alterations in the pathways controlling chromatin architecture (GO:0006325; Table 2) and Wnt signaling (GO:0016055) in both the skin and HG, the expression of two histone genes, *Hist1h2a1* and *Histh2af* (NM_178182 and NM_175661), as well as that of *Fzd10* (NM_175284; *Wnt frizzled receptor*), is augmented two- to threefold. Upregulation of the *Sfn* gene (NM_018754; *stratifin*) (34) is interesting, as the protein controls the keratinocyte proliferation/differentiation switch (56) and may be involved in the epidermal hypertrophy observed for *Aoh2*$^{-/-}$ mice (see below). Two genes suggesting that AOH2 deficiency is associated with alterations of the secretory phenotype not only in the HG but also in the skin are *Fgd1* (NM_008001) and *Sft2dr* (XM_484715). FGD1 is a Rho GTPase exchange factor whose deficit is at the basis of X-linked faciogenital dysplasia (24, 30). SFT2 is thought to be involved in vesicular transport in the Golgi compartment (21). Another gene of interest for its potential link to AOXs (64) in the same group is *Abcd2*

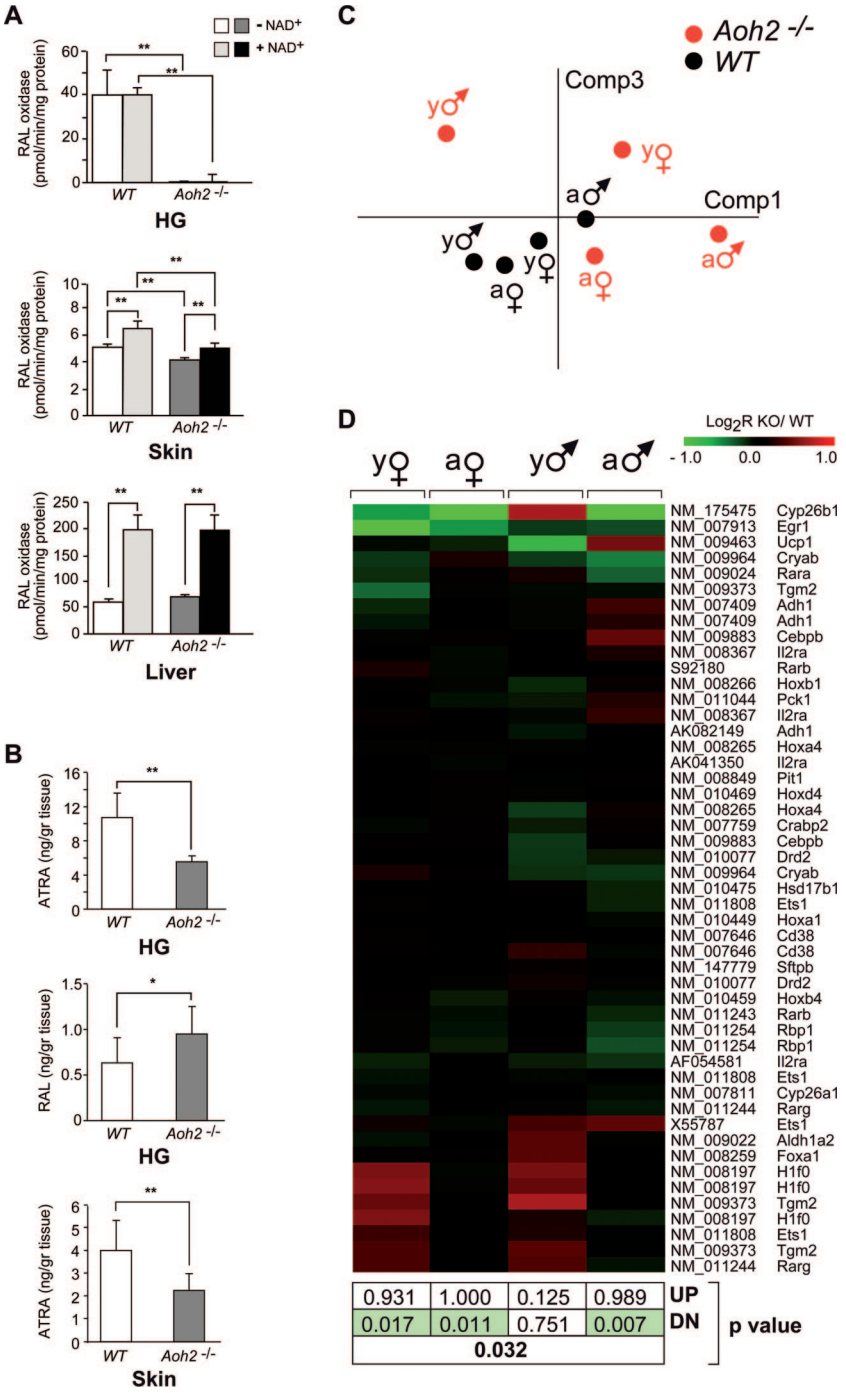

FIG. 7. AOH2-dependent oxidation of RAL in the HG and skin: effects on RAL/ATRA levels in vivo and gene expression correlates. (A) Cytosolic extracts were isolated from the indicated tissues of WT and *Aoh2*$^{-/-}$ mice depleted of NAD$^+$ by use of NAP-5 columns (GE Healthcare) and used to determine RAL-oxidizing activity in the absence or presence of readded nicotinamide cofactor. Each value is the mean ± standard deviation (SD) for three replicates. **, significantly different according to Student's *t* test ($P < 0.01$). The results are representative of at least two independent experiments performed on tissues from different batches of animals. (B) The amounts of RAL and ATRA were determined by LC-MS with the indicated tissues of WT and *Aoh2*$^{-/-}$ animals. Each value is the mean ± SD for four (RAL and HG) or eight (ATRA, HG, and skin) individual animals. **, significantly different according to Student's *t* test ($P < 0.01$). (C) Gene expression pattern of the retinoid-dependent genes in the HG. PCA of the VSN intensity values (means centered) in the eight experimental groups. Comp, component. (D) Heat map of the whole set of genes. The *P* values (upregulation [UP], downregulation [DN], or general significance in boldface) reported below the heat map refer to the GSEA, as described in Materials and Methods. This analysis was performed to demonstrate the prevalence of a decrease in the expression of retinoid-responsive genes (green boxes). Symbols: ♂, male; ♀, female. Abbreviations: a, adult; y, young; KO, knockout.

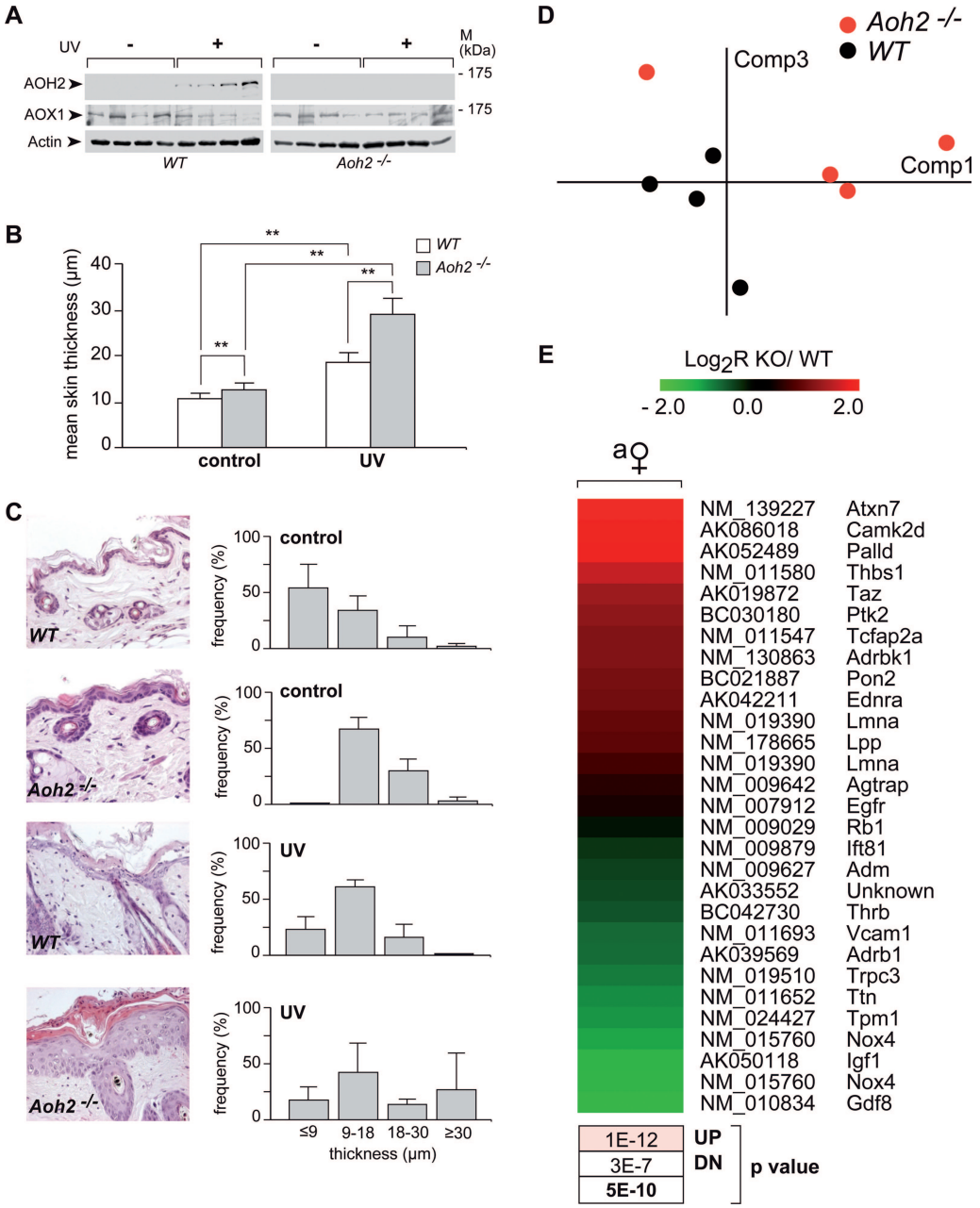

FIG. 8. Induction of AOH2 by UVB irradiation and epidermal hypertrophy in untreated and UVB-treated *Aoh2*$^{-/-}$ mice. Four WT or *Aoh2*$^{-/-}$ female mice per each experimental group were mock treated (control) or treated by UVB light irradiation on the dorsal area of the skin for 4 days, as described in Materials and Methods. (A) Skin biopsy samples of similar volumes were obtained from the same dorsal areas of the skin and homogenized. Homogenates (20 μg) were subjected to Western blot analysis with anti-AOH2, anti-AOX1, and anti-β-actin antibodies as indicated. Please note that in the Western blot shown, the lack of AOH2 signal in basal conditions is merely due to the low amount of total protein extract loaded. (B) The bar graph illustrates the results obtained on the thickness of the epidermal layer of the skin after serial morphometric analysis of the slides (25 fields per animal). **, significantly different (Student's *t* test, $P < 0.01$). M, molecular mass. (C) The micrographs show representative fields of the skin obtained from untreated (control) and UVB-irradiated (UV) WT or *Aoh2*$^{-/-}$ animals. The magnification of photographs is ×200. The right bar graphs show the distribution of the epidermal thicknesses after stratification in four discrete percentile classes. Each value is the mean ± SD for four animals. (D) Gene expression pattern of the tissue hypertrophy category (128 genes, 255 probes) in the skin. PCA of the VSN intensity values (means centered) in the eight samples. Comp, component. (E) Heat map of the genes significantly changed by AOH2 deletion ($P < 0.05$). The *P* values (upregulation[UP], downregulation[DN], or general significance in boldface) reported below the heat map refer to the GSEA, as described in Materials and Methods. This analysis was performed to demonstrate the prevalence of an increase in the expression of "hypertrophy" genes (reddish box). Symbols: ♀, female. Abbreviations: a, adult; y, young; KO, knockout.

TABLE 3. List of genes whose expression is significantly perturbed in the skin of *Aoh2*$^{-/-}$ mice[a]

Gene category	Accession no.	Gene name	logR[b]	*P* value[c]
Downregulated genes	AK147421	*Acsl6*	−1.81	1.74E–03
	AK050118	*Igf1*	−1.44	4.00E–03
	NM_033174	*Snurf*	−1.30	3.24E–03
	NM_013744	*Zfp354b*	−1.30	4.83E–03
	NM_022881	*Rgs18*	−1.27	2.60E–03
	NM_145713	*Hist1h1d*	−1.27	3.99E–03
	NM_011935	*Esrrg*	−1.27	7.15E–04
	NM_011670	*Uchl1*	−1.23	1.87E–03
	AY590892	*Dmxl1*	−1.19	2.02E–03
	NM_011994	*Abcd2*	−1.17	1.14E–03
	NM_030143	*Ddit4l*	−1.12	3.38E–03
	NM_026167	*Klhl13*	−1.08	1.92E–03
	NM_009808	*Casp12*	−1.05	4.50E–03
	AK029536	*Ttc18*	−1.03	4.98E–03
Downregulated unknown genes	NM_172419	9030612E09Rik	−1.55	3.27E–03
	BC058715	C030002C11Rik	−1.39	3.26E–03
	XM_126361	5730455P16Rik	−1.26	4.22E–03
	NM_027564	4921507P07Rik	−1.23	4.50E–03
	NM_001039244	LOC633640	−1.20	2.58E–03
	NM_172513	BC049806	−1.18	1.26E–03
	NM_172392	BC028265	−1.18	4.27E–03
	AK047247	AK047247	−1.15	2.40E–03
	XM_914237	LOC638271	−1.14	1.65E–03
	AK052002	AK052002	−1.08	1.84E–03
Upregulated genes	AK048375	*Mtap2*	3.80	8.07E–04
	AK089714	AK089714	3.04	1.32E–03
	AK018004	*Rps18*	2.71	3.74E–04
	XM_147798	*Slc4a7*	2.45	1.44E–03
	XM_900817	*Nrg1*	2.08	1.17E–03
	NM_010600	*Kcnh1*	2.04	4.59E–03
	AK045806	*Erbb2ip*	2.04	2.40E–03
	NM_175661	*Hist1h2af*	2.03	2.32E–03
	AK086235	*Wdr45l*	1.98	1.43E–03
	AK031473	*Polr3f*	1.97	3.98E–03
	AK090248	*Sec63*	1.97	2.65E–03
	NM_010110	*Efnb1*	1.86	4.35E–03
	AK080436	*Hmgn1*	1.75	1.36E–03
	NM_181820	*Tmc4*	1.74	4.05E–03
	AK172914	*Lpgat1*	1.67	1.55E–03
	NM_178182	*Hist1h2ai*	1.67	1.52E–03
	NM_178085	*Rab6ip2*	1.63	3.83E–03
	XM_132817	*Ankrd26*	1.58	4.60E–03
	AK040105	A430061O12Rik	1.56	1.03E–03
	NM_016871	*Tomm40*	1.51	3.93E–03
	TC1469302	TC1469302	1.49	2.49E–03
	AK044468	*Vps29*	1.48	2.53E–03
	AK082550	AK082550	1.45	4.52E–03
	AK037501	*Trpc4ap*	1.45	4.38E–03
	AK014632	*Mrpl38*	1.44	5.89E–04
	BC006644	*Smg6*	1.39	3.00E–03
	NM_028950	*Nsun6*	1.39	3.68E–03
	XM_484715	*Sft2d3*	1.36	2.09E–03
	AK045956	*Krit1*	1.35	4.27E–03
	NM_011119	*Pa2g4*	1.33	1.76E–03
	AK047982	*Rtn4*	1.33	1.60E–03
	NM_175284	*Fzd10*	1.28	2.21E–03
	NM_172266	*Lpgat1*	1.27	1.77E–03
	TC1414359	TC1414359	1.22	3.88E–03
	NM_153787	*Bclaf1*	1.20	2.87E–03
	XM_484715	*Sft2d3*	1.19	4.93E–03
	AK084917	*Rad23b*	1.12	3.16E–03
	NM_008001	*Fgd1*	1.12	1.86E–03
	NM_010792	*Mettl1*	1.11	1.39E–03
	NM_016775	*Dnajc5*	1.05	1.57E–03
	NM_029001	*Elovl7*	1.05	3.54E–03
	NM_009726	*Atp7a*	1.02	4.27E–03
	NM_018754	*Sfn*	1.01	2.64E–03
	NM_027026	*Lrrc46*	1.00	3.95E–03

Continued on following page

TABLE 3—*Continued*

Gene category	Accession no.	Gene name	logR[b]	*P* value[c]
Upregulated unknown genes	XM_912173	LOC636687	2.83	1.26E–03
	BC090402	BC090402	2.30	1.71E–03
	AK081758	B930068K11Rik	2.13	3.02E–03
	TC1477839	TC1477839	2.13	4.32E–03
	TC1522673	TC1522673	1.96	3.32E–03
	AK220358	9130404D08Rik	1.79	1.71E–03
	BC028769	6030458C11Rik	1.71	3.16E–03
	AK084691	AK084691	1.68	4.50E–03
	TC1533348	TC1533348	1.65	1.14E–03
	AK164650	5530601H04Rik	1.59	1.54E–03
	AK014787	4833428M15Rik	1.59	3.48E–03
	ENSMUST00000024982	ENSMUST00000024982	1.58	1.27E–03
	AK049426	AK049426	1.48	4.37E–03
	NM_177271	E130306M17Rik	1.46	4.24E–03
	AK081612	9130404D08Rik	1.46	3.08E–03
	AK011948	AK011948	1.43	9.84E–04
	AK036075	AK036075	1.42	2.90E–03
	AK013536	3010026O09Rik	1.38	2.09E–03
	NM_027561	4632415L05Rik	1.31	1.31E–03
	XM_923365	D430007A19Rik	1.23	3.08E–03
	NM_001012326	LOC433762	1.18	1.17E–03
	AK049476	C430014M02Rik	1.09	2.81E–03
	XM_130548	2610101J03Rik	1.04	3.13E–03
	AK079466	A030007N12Rik	1.00	2.67E–03

[a] List of the genes significantly up- or downregulated in the skin of *Aoh2*$^{-/-}$ mice after analysis of the gene expression microarray results ($P < 0.05$; >2-fold change).
[b] logR is the $\log_2$ ratio (*Aoh2*$^{-/-}$ versus WT mice) of the mean values for four individual pairs of animals.
[c] *P* values indicate the statistical significance of each determination.

(NM_011994), which is significantly downregulated and codes for a transporter protein belonging to the ABC transporter family.

Gene pathways altered in the skin of *Aoh2*$^{-/-}$ mice: similarities and differences with the HG. The same pathway analysis performed on the transcriptome of HGs was carried out with the skin data set (Table 2). In *Aoh2*$^{-/-}$ mice, we looked for the enrichment of pathways unique to the skin or in common with the HG. Out of the 59 pathways, 13 are specific for the skin (22%) and 23 (39%) are common to both. Among the common pathways, 13 are concordantly upregulated. As to the first group, we observed significant enrichment and an overall upregulation of the pathway controlling keratinocyte differentiation (GO:0030216). Overall downregulation of pathways involved in lymphocyte proliferation (GO:0050671), B-cell responses (GO:0030890; GO:0050871), and antigen presentation via major histocompatibility complex (GO:0019885) is also evident. Upregulation of the response to UV (GO:0009411) is of particular interest for the UV-irradiation-dependent phenotype observed in the skin of *Aoh2*$^{-/-}$ mice (see the next section).

As to the pathways in common between the skin and HG, Rho and Wnt signal transduction (GO:0007266, GO:0016055), vesicular trafficking (GO:0016192, GO:0045045, GO:0006897, GO:0048193), and ATPase activity (GO:0016887), consisting predominantly of ABC transporters, are of relevance. Although the observed enrichment of pathways like positive regulation of programmed cell death (GO:00043068) and microtubule-based process (GO:0007017) are listed as specific to the skin, they are linked to similar pathways also altered in the HG (GO:0043065 and GO:0000226). Along with the common pathways controlling cell projection and migration (GO:0042995 and GO:0016477), they may reflect tissue-remodeling processes accompanying epidermal hypertrophy.

Epidermal hypertrophy in the *Aoh2*$^{-/-}$ animal and gene expression correlates. Subchronic UVB irradiation of the skin is accompanied by induction of the AOH2 protein in WT animals (Fig. 8A). Induction is specific to AOH2, as expression of AOX1, the other AOX present in the skin, is not modified in the same experimental conditions. In addition, the elevation of AOH2 is due to direct exposure to UV light, as the levels of the protein are left unaffected in the HGs of irradiated animals (data not shown). All this indicates that induction of AOH2 is part of the response to UV activated in the skin. With this in mind, we studied the histological appearance of the tissue in *Aoh2*$^{-/-}$ animals not only under basal conditions but also after subchronic exposure to UV light. The UV experiments were also prompted by the microarray results shown in Table 2 indicating enrichment of the UV response pathway in the skin of *Aoh2*$^{-/-}$ mice.

Serial morphometric analysis of tissue sections obtained for basal conditions indicates that the overall thickness of the epidermal layer is significantly augmented in *Aoh2*$^{-/-}$ animals relative to what was seen for WT animals (Fig. 8B). The micrographs shown illustrate the point in two representative fields obtained from the dorsal skin (Fig. 8C, left). As the epidermal layer is heterogeneous and its thickness is position dependent, we looked at the distribution of the parameter in a large number of sections. In *Aoh2*$^{-/-}$ animals, we observed a shift toward the second and third quartiles of the epidermal thickness distribution (Fig. 8C, right). As expected, UV irradiation of WT animals results in a remarkable thickening not only of the epidermal but also of the dermal component of the skin (data not shown). A quantitative assessment of the in-

creased thickness of the epidermal layer is shown by the corresponding distribution graph. UV radiation-dependent thickening of the epidermis is enhanced in *Aoh2*$^{-/-}$ animals. In fact, the distribution graph shows a dramatic increase in the number of sections falling in the upper quartile.

Taken together, these results indicate that AOH2 acts as a negative modulator of the epidermal trophism. With respect to this, pathway analysis of the skin microarray data, with the use of the Metacore "diseases" lists rather than GO categories, resulted in the discovery of an interesting gene expression correlate. The top hit after comparison of the *Aoh2*$^{-/-}$ and WT datasets was the " tissue hypertrophy" category (128 genes, 255 probes). PCA of the genes contained in this category showed a clear separation between the *Aoh2*$^{-/-}$ and WT experimental samples (Fig. 8D). The heat map of the 29 individual genes whose expression is significantly altered as a consequence of AOH2 deletion shows a prevalence of upregulated genes (Fig. 8E). Most of the genes in the group have been studied in detail for their significance in myocardial hypertrophy. However, they may also exert a similar role in the epidermis, as their expression profile based on expressed sequence tag counts indicate that many of them are represented in the skin (UniGene resource at NCBI; http://www.ncbi.nlm.nih.gov/UniGene). Only a limited number of the corresponding protein products whose expression is significantly altered in *Aoh2*$^{-/-}$ mice will be considered. *Ataxin 7* (*Atxn7*) coding for a relatively ubiquitous protein, is at the top of the list of upregulated genes. Members of the ataxin family have recently been linked to tissue regeneration and epithelial cell repair in several organs, including the skin (52). The gene for the 2d form of calcium-calmodulin-dependent kinase II (*CaMKII2d*), a strong inducer of cardiac hypertrophy (19), may control keratinocyte proliferation and differentiation, which are calcium-dependent processes. As to *thrombospondin 1* (*Thbs1*), upregulation in *Aoh2*$^{-/-}$ mice may have an indirect role on epidermal hypertrophy, as the corresponding protein activates transforming growth factors, which are involved in controlling the proliferation of keratinocytes (69). The increase in the focal adhesion kinase gene, *Ptk2*, may just reflect the augmented number of keratinocytes in *Aoh2*$^{-/-}$ animals and the corresponding focal adhesions that keep these epithelial cells together. The transcription factor AP2 alpha (Tcfap2a) is present in the skin at relatively high levels and has a strong inductive effect on basal keratin expression (17). The gene for adrenergic receptor kinase, beta 1 (*Adrbk1*) regulates not only the proliferative state of various cell types but also the motility of epithelial cells (51). The downregulated myostatin gene (*Gdf8*) belongs to the transforming growth factor β family and is a negative regulator of muscle growth (32). Though expressed at high levels in the muscle and heart, myostatin is also present in the skin, where it could serve an antiproliferative effect on keratinocytes as well.

DISCUSSION

The data contained in this report provide novel insights into the tissue/cell distribution, biochemical characteristics, regulation, and function of AOH2, one of the four AOXs present in marsupials and rodents but absent from primates and humans (55). In particular, the generation and characterization of a constitutive *Aoh2* knockout mouse represents an important first step in the definition of the homeostatic function of the corresponding protein product, for which no information was available. The importance of this model is heightened by the fact that it is the first animal knockout targeting a member of the AOX family.

The tissue and cell distribution data indicate that by far the richest source of AOH2 is the HG. In this organ, AOH2 is the only member of the AOX family present, and it is very abundant, representing around 0.25% of all the cytosolic proteins. AOH2 is expressed by the main population of the secretory cells (14–16). Significant amounts of AOH2 are also evident in two prominent structures of the skin, i.e., the sebaceous glands and the suprabasal layer of the epidermis. The epidermis is not the sole keratinized epithelium where AOH2 is synthesized, as the protein is also present in the epithelial lining of the oral cavity, the esophagus, and the distal portion of the stomach (68).

AOH2 and the HG. The observation that mouse HGs are rich in AOH2 suggests that the enzyme exerts an important function in these structures. This organ-specific function must have become as dispensable as the entire gland in primates and humans (55), providing a simple explanation as to why the *Aoh2* orthologous gene was deleted from these two species. The HG develops predominantly after birth, becomes functionally mature in the adult, and is characterized by sexually dimorphic structural and biochemical traits (14–16). Different functions have been ascribed to the gland, such as lubrication and protection of the eye surface, control of the circadian rhythm, innate immunity, and the synthesis or secretion of pheromones regulating the sexual and social behavior of animals.

At present, the phenotypic studies conducted in *Aoh2*$^{-/-}$ mice do not provide any evidence for a role of AOH2 in the HG related to a protective effect on the eye. Indeed, the knockout mice do not show any sign of acute or chronic pathological alterations of the cornea or sclera. Similarly, behavioral studies aimed at evaluating an involvement of AOH2 in the control of circadian rhythm were substantially negative (Terao, unpublished). Incidentally, this observation suggests that AOH2 deficiency does not impinge on the synthesis of melatonin and porphyrins, which are the two main types of substances synthesized by the HGs and are purported to be involved in the control of circadian rhythm (14). At the transcriptomic level, this is supported by lack of perturbations in the expression of genes participating in the biosynthetic/catabolic pathways of melatonin or porphyrins. Though ad hoc studies on mating and social behaviors have not been conducted, observations of *Aoh2*$^{-/-}$ animals have been against a role for AOH2 in these two types of activity largely controlled by pheromones. Obviously, our animal colonies are bred and maintained in standard-pathogen-free animal house facilities under standard conditions. Thus, our observations do not rule out the possible relevance of the enzyme in the synthesis/catabolism or secretion/absorption of pheromones by the HG when the animals are exposed to stronger environmental stimuli. The transcriptome profiling experiments and subsequent pathway analyses indicate that the major perturbations afforded by *Aoh2* deletion are observed in young animals, suggesting that AOH2 is implicated predominantly in the struc-

tural and functional maturation of the gland. Interestingly, our microarray data suggest that the transcriptome of young females is affected by *Aoh2* deletion more significantly than is the male counterpart. This may be linked to the observed negative effect of endogenous testosterone on AOH2 expression (Fig. 3C and D). In the adult, the function of AOH2 may become more restricted, with more subtle overall consequences in terms of transcriptome perturbations. At least partially, this may be the result of unidentified compensatory mechanisms, which, however, do not include transcriptional activation of the genes coding for other aldehyde isoenzymatic forms (data not shown).

A potential mediator of the effects exerted by AOH2 in both immature and mature mice is ATRA. In fact, RAL, the physiological precursor of ATRA, is an excellent substrate of purified AOH2. Furthermore, AOH2 is responsible for the majority of the HGs' enzymatic activity transforming RAL into ATRA. In this site, AOH2 seems to be much more important than RALDHs (Raldh1, Raldh2, and Raldh3) in the synthesis of ATRA from RAL (45). Finally, the HGs of *Aoh2*$^{-/-}$ mice are characterized by increases in the basal levels of RAL and a corresponding decrease in the amounts of ATRA. All this is consistent with a role for AOH2 in regulating the local synthesis of ATRA. Although the quantitative reduction of ATRA in the HGs of knockout animals is approximately twofold, the effect is likely to be of physiological relevance, as it is accompanied by a significant overall downregulation of the small group of genes, which are established and direct retinoid targets (5).

How do alterations in the local levels of ATRA or possibly RAL relate to the suggested changes in the development and transcriptomic profile of the HG observed for *Aoh2*$^{-/-}$ animals? ATRA is a well-known morphogen controlling the development of multiple organs and systems in the embryo. This may explain why the major perturbations in the transcriptome afforded by *Aoh2* deletion are observed in sexually immature animals of both sexes. The phenomenon may be related to a potential role of AOH2 in the postnatal development of the HG via control of ATRA in a spatially and temporally restricted fashion. Interestingly, *Raldh3* knockout mice show atresia of the HG (22), demonstrating that the enzyme is important for the genesis of this organ in the embryo. We propose that AOH2 takes the place of Raldh3 after birth. Besides its developmental effects, ATRA is particularly important in the control of epithelial cells' homeostasis and is a purported modulator of HGs' function (74). In addition, the HG is a major deposit of ATRA after administration of the radioactive compound to vitamin A-deficient mice (75). Alterations in pathways controlling cell proliferation and death/survival, transcription/translation, chromatin structure, and cytoskeletal organization may simply reflect a tissue-remodeling effect due to perturbations of local and AOH2-dependent ATRA synthesis. In this context, the enrichment of the Wnt/β-catenin pathway is of relevance, as ATRA is known to exert numerous modulating effects on this signal transduction system (26, 27).

There is support in the literature for the possible influence that ATRA or RAL has on vital and specific functions of the HG's epithelial cells, like cellular secretion and lipid homeostasis (3). As to the first aspect, the literature is rich in studies on the role exerted by retinoids on the function of exocrine glands and sebaceous glands in particular (58, 73). With respect to lipids, ATRA has been recently shown to activate not only the classic rexinoid/retinoic acid receptors but also peroxisome proliferator-activated receptors α/β (20, 59, 60, 63), which are major positive regulators of lipid/cholesterol biosynthesis and accumulation (62). There is increasing evidence that RAL is not simply a precursor of ATRA but is on its own an important negative modulator of lipid biosynthesis and adipocyte differentiation (76, 77). No matter whether ATRA or RAL forms the basis of the perturbations in lipid homeostasis-controlling genes observed for *Aoh2*$^{-/-}$ mice, the expected net result would be the same, i.e., an antilipidemic or anticholesterolemic effect. In line with this expectation, preliminary experiments demonstrate a decrease in the amounts of cholesterol extracted from the HGs of *Aoh2*$^{-/-}$ animals (Terao, unpublished observations, 2008).

AOH2 and the skin. In the skin, AOH2 is synthesized by two main structures, the sebaceous glands, which are located in the dermis, and the suprabasal layer of the epidermis. Sebaceous glands and HGs share many similarities. They are both exocrine glands, producing a lipid-rich secretion; have similar secretory modalities; are involved in the production/secretion of pheromones; and accumulate significant amounts of retinoids (39). Sebaceous glands and the epidermis cooperate in providing a lipid-containing barrier to the penetration of environmental chemicals by limiting their diffusion to the skin (40). In addition, the suprabasal layer of epidermis and the sebaceous gland contain the highest levels of retinoids in the skin (1).

As already discussed in the case of the HG, a fundamental question strictly related to the function of AOH2 in sebaceous glands and epidermis is why the enzyme became obsolete in primates and humans. Indeed, the two skin structures are conserved in rodents, primates, and humans. One possible and partial answer relates to the fact that mammalian sebaceous glands are known to control thermoregulation via secretion of thermally insulating lipids (incidentally, the same is proposed for the HG). This function in humans is essentially different from that in other mammals, which are adapted to respond much more promptly to environmental changes of temperature. It may be envisaged that AOH2 serves a role in the rapid activation/inactivation of chemical signals or hormones controlling the secretion of lipids. The human organism may have evolved different chemical mediators that are no longer substrates of AOH2. Another and more comprehensive answer stems from our observation that AOH2 is not the only AOX present in the skin, as the expression of AOX1 is also evident (Fig. 8A). AOX1 is the only active AOX present in primates and humans, and there is evidence for the expression of the corresponding gene in human skin (UniGene Hs.406238). Human and mouse AOX1 proteins share common substrates with AOH2, including RAL (Terao, unpublished results, 2008). Thus, it is possible that the rodent skin is a more robust system than the primate/human counterpart and requires redundancy in AOXs. In humans and primates, it is possible that a single AOX is enough. Interestingly, we showed that AOH2 is inducible upon application of external stimuli like UV, while AOX1 is not, suggesting that the function exerted by the former protein is particularly important in stressful conditions.

In spite of a low overall level of AOH2 expression, skin is presently the only organ of *Aoh2*$^{-/-}$ mice characterized by a

morphologically recognizable alteration in the phenotype. Increased thickness of the *Aoh2*$^{-/-}$ epidermis is maintained after exposure to UV light, an external stimulus inducing an epidermal hypertrophic response on its own. Analysis of the skin transcriptome of *Aoh2*$^{-/-}$ animals is consistent with the observed phenotype and shows a number of significant alterations in general pathways controlling cell proliferation, death/survival, motility, cytoskeletal structure, tissue remodeling, and, finally, hypertrophy. This is accompanied by perturbations of additional specific and relevant pathways like keratinocyte differentiation, Wnt signaling, and response to UV. Interestingly, keratinocyte differentiation and response to UV are pathways specifically enriched in the skin relative to the HG.

As in the case of the HG, is it possible to link the morphological and transcriptomic alterations observed for the *Aoh2*$^{-/-}$ mice with the reported influence of AOH2 on the levels of ATRA in the skin? Measurement of ATRA levels in *Aoh2*$^{-/-}$ mice indicates a role for AOH2 in the homeostasis of vitamin A in the skin, although the enzyme's contribution to total RAL-oxidizing activity is lower in this organ than in the HG. It is well known that vitamin A deficiency is associated with extensive proliferation of epithelial cells in various organs, including the skin. The epidermal hypertrophy of *Aoh2*$^{-/-}$ animals is also reminiscent of that observed for a line of transgenic animals characterized by the expression of a dominant negative form of the retinoid receptor, RARα (4). This last animal model is characterized by hyperkeratosis and scaling in addition to skin lipid dystrophy. Hence, our findings are consistent with the concept that *Aoh2* deletion causes local ATRA deficiency and the ensuing epidermal hypertrophy.

At present, it is not possible to know whether the observed effect on the epidermis is the result of a direct action on keratinocytes caused by retinoid deficiency or if more-complex underlying mechanisms are operative. In fact, the action of ATRA on the growth and trophism of epidermal keratinocytes is controversial. ATRA inhibits the growth of keratinocytes in vitro, while the external application of high doses of retinoids seems to have the opposite effect in vivo (23, 57). For instance, it is entirely possible that epidermal hypertrophy is a secondary response to alteration in the homeostasis of the immune system triggered by local ATRA deficiency, as suggested by pathway analysis of the microarray data. ATRA is a well-known modulator of the immune system, and alteration of the homeostasis of the skin immune responses could influence the growth of the epidermal layer, altering the balance of cytokines and growth factors secreted by lymphocytes and/or macrophages (1).

Retinoid-related versus -unrelated functions of AOH2. In conclusion, many of the data obtained in the knockout model described in this report are consistent with a significant role of AOH2 in the local synthesis and biodisposition of endogenous retinoids in the HG and skin. If this is indeed the case, it must be emphasized that the role of AOH2 is not systemic and is limited to a few target organs and to the adult organism. This is in line with a multimodal and complex control of the homeostasis of endogenous retinoids. In this scenario, Raldh1, Raldh2, and Raldh3 are certainly more important than AOH2 in regulating the systemic levels of endogenous retinoids and the function of vitamin A in organogenesis and embryo development. The significance of AOH2 for retinoid homeostasis does not rule out functions and substrates other than RAL for AOH2. AOH2 may protect the skin and the body via metabolism of harmful exogenous compounds. The hypothesis will be easy to test in vivo by determining the sensitivity of our knockout animals to selected environmental poisons or pollutants. However, a prerequisite for this type of studies is a better definition of the exogenous substrates of AOH2 to determine whether the enzyme has the same broad specificity that characterizes other AOXs. In addition, it is possible that some of these alternative functions may be unrelated to the enzymatic activity of AOH2, as observed in the case of the other molybdoflavoenzyme, XOR (71). With respect to this, the recent reports demonstrating that human AOX1 is capable of interacting with ABC transporters and is important for the accumulation of triglycerides through as-yet-undefined mechanisms (72) are of great relevance for the presence of AOH2 in both HGs and sebaceous glands.

ACKNOWLEDGMENTS

This work was partially supported by unrestricted grants from FIRB (Fondo Italiano per la Ricerca di Base to M.T.), Fondazione Italo Monzino (to E.G.), and Fondazione Telethon (B055FIRB to C.T.).

We thank Mario Salmona for critical reading of the manuscript. The help of Felice Deceglie and Alessandro Soave for the artwork is also acknowledged.

REFERENCES

1. **Alique, M., F. J. Lucio-Cazana, V. Moreno, Q. Xu, T. Konta, K. Nakayama, A. Furusu, J. C. Sepulveda, and M. Kitamura.** 2007. Upregulation of cyclooxygenases by retinoic acid in rat mesangial cells. Pharmacology **79:**57–64.
2. **Al-Salmy, H. S.** 2001. Individual variation in hepatic aldehyde oxidase activity. IUBMB Life **51:**249–253.
3. **Anzano, M. A., A. J. Lamb, and J. A. Olson.** 1981. Impaired salivary gland secretory function following the induction of rapid, synchronous vitamin A deficiency in rats. J. Nutr. **111:**496–504.
4. **Attar, P. S., P. W. Wertz, M. McArthur, S. Imakado, J. R. Bickenbach, and D. R. Roop.** 1997. Inhibition of retinoid signaling in transgenic mice alters lipid processing and disrupts epidermal barrier function. Mol. Endocrinol. **11:**792–800.
5. **Balmer, J. E., and R. Blomhoff.** 2002. Gene expression regulation by retinoic acid. J. Lipid Res. **43:**1773–1808.
6. **Beedham, C.** 1987. Molybdenum hydroxylases: biological distribution and substrate-inhibitor specificity. Prog. Med. Chem. **24:**85–127.
7. **Beedham, C.** 1997. The role of non-P450 enzymes in drug oxidation. Pharm. World Sci. **19:**255–263.
8. **Beedham, C., Y. al-Tayib, and J. A. Smith.** 1992. Role of guinea pig and rabbit hepatic aldehyde oxidase in oxidative in vitro metabolism of cinchona antimalarials. Drug Metab. Dispos. **20:**889–895.
9. **Beedham, C., S. E. Bruce, and D. J. Rance.** 1987. Tissue distribution of the molybdenum hydroxylases, aldehyde oxidase and xanthine oxidase, in male and female guinea pigs. Eur. J. Drug Metab. Pharmacokinet. **12:**303–306.
10. **Beedham, C., J. J. Miceli, and R. S. Obach.** 2003. Ziprasidone metabolism, aldehyde oxidase, and clinical implications. J. Clin. Psychopharmacol. **23:**229–232.
11. **Beedham, C., C. F. Peet, G. I. Panoutsopoulos, H. Carter, and J. A. Smith.** 1995. Role of aldehyde oxidase in biogenic amine metabolism. Prog. Brain Res. **106:**345–353.
12. **Bendotti, C., E. Prosperini, M. Kurosaki, E. Garattini, and M. Terao.** 1997. Selective localization of mouse aldehyde oxidase mRNA in the choroid plexus and motor neurons. Neuroreport **8:**2343–2349.
13. **Berger, R., E. Mezey, K. P. Clancy, G. Harta, R. M. Wright, J. E. Repine, R. H. Brown, M. Brownstein, and D. Patterson.** 1995. Analysis of aldehyde oxidase and xanthine dehydrogenase/oxidase as possible candidate genes for autosomal recessive familial amyotrophic lateral sclerosis. Somat. Cell Mol. Genet. **21:**121–131.
14. **Buzzell, G. R.** 1996. The Harderian gland: perspectives. Microsc. Res. Tech. **34:**2–5.
15. **Buzzell, G. R.** 1996. Sexual dimorphism in the Harderian gland of the Syrian hamster is controlled and maintained by hormones, despite seasonal fluctuations in hormone levels: functional implications. Microsc. Res. Tech. **34:**133–138.
16. **Buzzell, G. R., J. L. Blank, M. K. Vaughan, and R. J. Reiter.** 1995. Control of secretory lipid droplets in the Harderian gland by testosterone and the

photoperiod: comparison of two species of hamsters. Gen. Comp. Endocrinol. **99:**230–238.
17. **Byrne, C., M. Tainsky, and E. Fuchs.** 1994. Programming gene expression in developing epidermis. Development **120:**2369–2383.
18. **Chambon, P.** 1996. A decade of molecular biology of retinoic acid receptors. FASEB J. **10:**940–954.
19. **Chang, L., J. Zhang, Y. H. Tseng, C. Q. Xie, J. Ilany, J. C. Bruning, Z. Sun, X. Zhu, T. Cui, K. A. Youker, Q. Yang, S. M. Day, C. R. Kahn, and Y. E. Chen.** 2007. Rad GTPase deficiency leads to cardiac hypertrophy. Circulation **116:**2976–2983.
20. **Chou, C. F., C. L. Lai, Y. C. Chang, G. Duester, and S. J. Yin.** 2002. Kinetic mechanism of human class IV alcohol dehydrogenase functioning as retinol dehydrogenase. J. Biol. Chem. **277:**25209–25216.
21. **Conchon, S., X. Cao, C. Barlowe, and H. R. Pelham.** 1999. Got1p and Sft2p: membrane proteins involved in traffic to the Golgi complex. EMBO J. **18:**3934–3946.
22. **Dupe, V., N. Matt, J. M. Garnier, P. Chambon, M. Mark, and N. B. Ghyselinck.** 2003. A newborn lethal defect due to inactivation of retinaldehyde dehydrogenase type 3 is prevented by maternal retinoic acid treatment. Proc. Natl. Acad. Sci. USA **100:**14036–14041.
23. **Fisher, G. J., and J. J. Voorhees.** 1996. Molecular mechanisms of retinoid actions in skin. FASEB J. **10:**1002–1013.
24. **Gao, J., L. Estrada, S. Cho, R. E. Ellis, and J. L. Gorski.** 2001. The Caenorhabditis elegans homolog of FGD1, the human Cdc42 GEF gene responsible for faciogenital dysplasia, is critical for excretory cell morphogenesis. Hum. Mol. Genet. **10:**3049–3062.
25. **Garattini, E., M. Fratelli, and M. Terao.** 2008. Mammalian aldehyde oxidases: genetics, evolution and biochemistry. Cell. Mol. Life Sci. **65:**1019–1048.
26. **Garattini, E., M. Gianni, and M. Terao.** 2007. Cytodifferentiation by retinoids, a novel therapeutic option in oncology: rational combinations with other therapeutic agents. Vitam. Horm. **75:**301–354.
27. **Garattini, E., M. Gianni, and M. Terao.** 2007. Retinoids as differentiating agents in oncology: a network of interactions with intracellular pathways as the basis for rational therapeutic combinations. Curr. Pharm. Des. **13:**1375–1400.
28. **Garattini, E., R. Mendel, M. J. Romao, R. Wright, and M. Terao.** 2003. Mammalian molybdo-flavoenzymes, an expanding family of proteins: structure, genetics, regulation, function and pathophysiology. Biochem. J. **372:**15–32.
29. **Huber, W., A. von Heydebreck, H. Sultmann, A. Poustka, and M. Vingron.** 2002. Variance stabilization applied to microarray data calibration and to the quantification of differential expression. Bioinformatics **18**(Suppl. 1)**:**S96–S104.
30. **Ito, K., T. Suzuki, T. Moriya, H. Utsunomiya, A. Sugawara, R. Konno, S. Sato, and H. Sasano.** 2001. Retinoid receptors in the human endometrium and its disorders: a possible modulator of 17 beta-hydroxysteroid dehydrogenase. J. Clin. Endocrinol. Metab. **86:**2721–2727.
31. **Jeyaraj, D. A., G. Grossman, and P. Petrusz.** 2005. Altered bioavailability of testosterone in androgen-binding protein-transgenic mice. Steroids **70:**704–714.
32. **Joulia-Ekaza, D., and G. Cabello.** 2007. The myostatin gene: physiology and pharmacological relevance. Curr. Opin. Pharmacol. **7:**310–315.
33. **Joyner, A. L.** 2000. Gene targeting: a practical approach, 2nd ed. Oxford University Press, Oxford, United Kingdom.
34. **Kilani, R. T., A. Medina, A. Aitken, R. B. Jalili, M. Carr, and A. Ghahary.** 2008. Identification of different isoforms of 14-3-3 protein family in human dermal and epidermal layers. Mol. Cell. Biochem. **314:**161–169.
35. **Kundu, T. K., R. Hille, M. Velayutham, and J. L. Zweier.** 2007. Characterization of superoxide production from aldehyde oxidase: an important source of oxidants in biological tissues. Arch. Biochem. Biophys. **460:**113–121.
36. **Kurosaki, M., S. Demontis, M. M. Barzago, E. Garattini, and M. Terao.** 1999. Molecular cloning of the cDNA coding for mouse aldehyde oxidase: tissue distribution and regulation in vivo by testosterone. Biochem. J. **341:**71–80.
37. **Kurosaki, M., M. Terao, M. M. Barzago, A. Bastone, D. Bernardinello, M. Salmona, and E. Garattini.** 2004. The aldehyde oxidase gene cluster in mice and rats. Aldehyde oxidase homologue 3, a novel member of the molybdo-flavoenzyme family with selective expression in the olfactory mucosa. J. Biol. Chem. **279:**50482–50498.
38. **Lee, H. K., W. Braynen, K. Keshav, and P. Pavlidis.** 2005. ErmineJ: tool for functional analysis of gene expression data sets. BMC Bioinformatics **6:**269.
39. **Madani, K. A., G. S. Bazzano, and A. C. Chou.** 1985. The in vitro metabolism of 13-cis-retinoic acid in a model sebaceous structure, the rat preputial gland. J. Investig. Dermatol. **85:**465–469.
40. **Madison, K. C.** 2003. Barrier function of the skin: "la raison d'etre" of the epidermis. J. Investig. Dermatol. **121:**231–241.
41. **Majkic-Singh, N., B. Conteh, M. Stojanov, and I. Berkes.** 1983. Kinetic assay of aldehyde oxidase with 2,2′-azino-di-(3-ethylbenzthiazoline-6-sulfonate) as chromogen. Enzyme **29:**120–125.
42. **Mira, L., L. Maia, L. Barreira, and C. F. Manso.** 1995. Evidence for free radical generation due to NADH oxidation by aldehyde oxidase during ethanol metabolism. Arch. Biochem. Biophys. **318:**53–58.
43. **Molotkov, A., and G. Duester.** 2003. Genetic evidence that retinaldehyde dehydrogenase Raldh1 (Aldh1a1) functions downstream of alcohol dehydrogenase Adh1 in metabolism of retinol to retinoic acid. J. Biol. Chem. **278:**36085–36090.
44. **Nagy, A., M. Gertsenstein, K. Vintersten, and R. Behringer.** 2003. Manipulating the mouse embryo, 3rd ed. Cold Spring Harbor Laboratory Press, Cold Spring Harbor, NY.
45. **Niederreither, K., and P. Dolle.** 2008. Retinoic acid in development: towards an integrated view. Nat. Rev. Genet. **9:**541–553.
46. **Nishimura, M., and S. Naito.** 2006. Tissue-specific mRNA expression profiles of human phase I metabolizing enzymes except for cytochrome P450 and phase II metabolizing enzymes. Drug Metab. Pharmacokinet. **21:**357–374.
47. **Okada, K., H. R. Lijnen, M. Dewerchin, A. Belayew, O. Matsuo, D. Collen, and R. Bernaerts.** 1997. Characterization and targeting of the murine alpha2-antiplasmin gene. Thromb. Haemost. **78:**1104–1110.
48. **Panoutsopoulos, G. I., and C. Beedham.** 2004. Kinetics and specificity of guinea pig liver aldehyde oxidase and bovine milk xanthine oxidase towards substituted benzaldehydes. Acta Biochim. Pol. **51:**649–663.
49. **Panoutsopoulos, G. I., D. Kouretas, and C. Beedham.** 2004. Contribution of aldehyde oxidase, xanthine oxidase, and aldehyde dehydrogenase on the oxidation of aromatic aldehydes. Chem. Res. Toxicol. **17:**1368–1376.
50. **Panoutsopoulos, G. I., D. Kouretas, E. G. Gounaris, and C. Beedham.** 2004. Metabolism of 2-phenylethylamine and phenylacetaldehyde by precision-cut guinea pig fresh liver slices. Eur. J. Drug Metab. Pharmacokinet. **29:**111–118.
51. **Penela, P., C. Ribas, I. Aymerich, N. Eijkelkamp, O. Barreiro, C. J. Heijnen, A. Kavelaars, F. Sanchez-Madrid, and F. Mayor, Jr.** 2008. G protein-coupled receptor kinase 2 positively regulates epithelial cell migration. EMBO J. **27:**1206–1218.
52. **Pogach, M. S., Y. Cao, G. Millien, M. I. Ramirez, and M. C. Williams.** 2007. Key developmental regulators change during hyperoxia-induced injury and recovery in adult mouse lung. J. Cell. Biochem. **100:**1415–1429.
53. **Rashidi, M. R., C. Beedham, J. S. Smith, and S. Davaran.** 2007. In vitro study of 6-mercaptopurine oxidation catalysed by aldehyde oxidase and xanthine oxidase. Drug Metab. Pharmacokinet. **22:**299–306.
54. **Rashidi, M. R., J. A. Smith, S. E. Clarke, and C. Beedham.** 1997. In vitro oxidation of famciclovir and 6-deoxypenciclovir by aldehyde oxidase from human, guinea pig, rabbit, and rat liver. Drug Metab. Dispos. **25:**805–813.
55. **Rehorek, S. J., and T. D. Smith.** 2006. The primate Harderian gland: does it really exist? Ann. Anat. **188:**319–327.
56. **Richardson, R. J., J. Dixon, S. Malhotra, M. J. Hardman, L. Knowles, R. P. Boot-Handford, P. Shore, A. Whitmarsh, and M. J. Dixon.** 2006. Irf6 is a key determinant of the keratinocyte proliferation-differentiation switch. Nat. Genet. **38:**1329–1334.
57. **Rittie, L., J. Varani, S. Kang, J. J. Voorhees, and G. J. Fisher.** 2006. Retinoid-induced epidermal hyperplasia is mediated by epidermal growth factor receptor activation via specific induction of its ligands heparin-binding EGF and amphiregulin in human skin in vivo. J. Investig. Dermatol. **126:**732–739.
58. **Schirren, C. G., T. Jansen, A. Lindner, P. Kind, and G. Plewig.** 1996. Diffuse sebaceous gland hyperplasia. A case report and an immunohistochemical study with cytokeratins. Am. J. Dermatopathol. **18:**296–301.
59. **Schug, T. T., D. C. Berry, N. S. Shaw, S. N. Travis, and N. Noy.** 2007. Opposing effects of retinoic acid on cell growth result from alternate activation of two different nuclear receptors. Cell **129:**723–733.
60. **Schug, T. T., D. C. Berry, I. A. Toshkov, L. Cheng, A. Y. Nikitin, and N. Noy.** 2008. Overcoming retinoic acid-resistance of mammary carcinomas by diverting retinoic acid from PPARbeta/delta to RAR. Proc. Natl. Acad. Sci. USA **105:**7546–7551.
61. **Schwab, S. R., J. P. Pereira, M. Matloubian, Y. Xu, Y. Huang, and J. G. Cyster.** 2005. Lymphocyte sequestration through S1P lyase inhibition and disruption of S1P gradients. Science **309:**1735–1739.
62. **Semple, R. K., V. K. Chatterjee, and S. O'Rahilly.** 2006. PPAR gamma and human metabolic disease. J. Clin. Investig. **116:**581–589.
63. **Shaw, N., M. Elholm, and N. Noy.** 2003. Retinoic acid is a high affinity selective ligand for the peroxisome proliferator-activated receptor beta/delta. J. Biol. Chem. **278:**41589–41592.
64. **Sigruener, A., C. Buechler, E. Orso, A. Hartmann, P. J. Wild, L. Terracciano, M. Roncalli, S. R. Bornstein, and G. Schmitz.** 2007. Human aldehyde oxidase 1 interacts with ATP-binding cassette transporter-1 and modulates its activity in hepatocytes. Horm. Metab. Res. **39:**781–789.
65. **Terao, M., M. Kurosaki, M. M. Barzago, E. Varasano, A. Boldetti, A. Bastone, M. Fratelli, and E. Garattini.** 2006. Avian and canine aldehyde oxidases. Novel insights into the biology and evolution of molybdo-flavoenzymes. J. Biol. Chem. **281:**19748–19761.
66. **Terao, M., M. Kurosaki, S. Demontis, S. Zanotta, and E. Garattini.** 1998. Isolation and characterization of the human aldehyde oxidase gene: conservation of intron/exon boundaries with the xanthine oxidoreductase gene indicates a common origin. Biochem. J. **332:**383–393.
67. **Terao, M., M. Kurosaki, M. Marini, M. A. Vanoni, G. Saltini, V. Bonetto, A. Bastone, C. Federico, S. Saccone, R. Fanelli, M. Salmona, and E. Garattini.**

2001. Purification of the aldehyde oxidase homolog 1 (AOH1) protein and cloning of the AOH1 and aldehyde oxidase homolog 2 (AOH2) genes. Identification of a novel molybdo-flavoprotein gene cluster on mouse chromosome 1. J. Biol. Chem. **276:**46347–46363.

68. **Terao, M., M. Kurosaki, G. Saltini, S. Demontis, M. Marini, M. Salmona, and E. Garattini.** 2000. Cloning of the cDNAs coding for two novel molybdo-flavoproteins showing high similarity with aldehyde oxidase and xanthine oxidoreductase. J. Biol. Chem. **275:**30690–30700.
69. **Vassar, R., and E. Fuchs.** 1991. Transgenic mice provide new insights into the role of TGF-alpha during epidermal development and differentiation. Genes Dev. **5:**714–727.
70. **Vila, R., M. Kurosaki, M. M. Barzago, M. Kolek, A. Bastone, L. Colombo, M. Salmona, M. Terao, and E. Garattini.** 2004. Regulation and biochemistry of mouse molybdo-flavoenzymes. The DBA/2 mouse is selectively deficient in the expression of aldehyde oxidase homologues 1 and 2 and represents a unique source for the purification and characterization of aldehyde oxidase. J. Biol. Chem. **279:**8668–8683.
71. **Vorbach, C., A. Scriven, and M. R. Capecchi.** 2002. The housekeeping gene xanthine oxidoreductase is necessary for milk fat droplet enveloping and secretion: gene sharing in the lactating mammary gland. Genes Dev. **16:** 3223–3235.
72. **Weigert, J., M. Neumeier, S. Bauer, W. Mages, A. A. Schnitzbauer, A. Obed, B. Groschl, A. Hartmann, A. Schaffler, C. Aslanidis, J. Scholmerich, and C. Buechler.** 2008. Small-interference RNA-mediated knock-down of aldehyde oxidase 1 in 3T3-L1 cells impairs adipogenesis and adiponectin release. FEBS Lett. **582:**2965–2972.
73. **Wrobel, A., H. Seltmann, S. Fimmel, K. Muller-Decker, M. Tsukada, B. Bogdanoff, N. Mandt, U. Blume-Peytavi, C. E. Orfanos, and C. C. Zouboulis.** 2003. Differentiation and apoptosis in human immortalized sebocytes. J. Investig. Dermatol. **120:**175–181.
74. **Zhuang, Y. H., M. Blauer, M. Pelto-Huikko, H. Syvala, and P. Tuohimaa.** 1996. Immunochemical and in situ hybridization analyses of retinoic acid receptor alpha, beta, and gamma in murine Harderian and submandibular glands. Histochem. Cell Biol. **106:**311–318.
75. **Zhuang, Y. H., E. L. Sainio, P. Sainio, W. V. Vedeckis, T. Ylikomi, and P. Tuohimaa.** 1995. Distribution of all-trans-retinoic acid in normal and vitamin A deficient mice: correlation to retinoic acid receptors in different tissues of normal mice. Gen. Comp. Endocrinol. **100:**170–178.
76. **Ziouzenkova, O., G. Orasanu, M. Sharlach, T. E. Akiyama, J. P. Berger, J. Viereck, J. A. Hamilton, G. Tang, G. G. Dolnikowski, S. Vogel, G. Duester, and J. Plutzky.** 2007. Retinaldehyde represses adipogenesis and diet-induced obesity. Nat. Med. **13:**695–702.
77. **Ziouzenkova, O., and J. Plutzky.** 2008. Retinoid metabolism and nuclear receptor responses: new insights into coordinated regulation of the PPAR-RXR complex. FEBS Lett. **582:**32–38.